DESIGN AND CONSTRUCTION OF A POINT-FOCUSING BERREMAN TYPE SINGLE CRYSTAL X-RAY MONOCHROMATOR AND ITS APPLICATION TO LOW-ANGLE SCATTERING STUDIES OF BIOLOGICAL SPECIMENS

Thesis by

William Edwin Dibble

In Partial Fulfillment of the Requirements

For the Degree of

Doctor of Philosophy

California Institute of Technology

Pasadena, California

1960

ACKNOWLEDGMENTS

The author wishes to express his deep appreciation of the continuing guidance and assistance of his thesis supervisor, Professor Jesse W. M. DuMond, during the entire period of work reported in this thesis, and also of financial support from the United States Atomic Energy Commission.

The author is indebted to Dr. Dwight W. Berreman who introduced him to the field of low-angle X-ray scattering, to Dr. Don Caspar, who suggested examination of the ribosome particles, for his constant interest in the project, and to Dr. Howard M. Dintzis and Dr. Paul O. P. T'so who supplied the ribosome particles and valuable assistance in the interpretation of results. The author also wishes to thank Dr. Don Ridgeway and Dr. Jerome Vinograd for their assistance and cooperation in this and related projects.

The assistance of Mr. Harold T. Yura is gratefully acknowledged in the design, construction, and data handling of the project. Thanks are also due to Mr. Alfred W. Doering for construction of the collimator, to the staff of the central shop facilities of the Institute who aided in the construction of the instrument, and to Mr. Douglas Marlow for consultation on the design of the instrument.

The Berreman point-focusing monochromator is a patented device under U. S. Letters Patent 2,853,617 issued September 23, 1958, and assigned to the California Institute Research Foundation for exploitation. Use was made of this device with permission of the California Institute Research Foundation.

ABSTRACT

The design and construction of a point-focusing Berreman type single quartz crystal X-ray monochromator is described. Monochromatization and point focusing of the copper $K\alpha_1$ line are obtained by Bragg reflection from the surface of a 2 1/2 by 2 3/8 by 0.015 in. curved crystal lamina which has been subjected to two successive cylindrical bendings at right angles to each other. With a 0.0225 in. aperture defining the size of the X-ray source next to a General Electric CA-7 diffraction tube running at 45 KV and 18 ma, about 3×10^9 counts per minute as determined by Geiger tube measurements may be put into a 0.025 half width focus, with the beam in helium atmosphere. Parasitic scattering from the crystal had to be excluded by using a converging vane collimator, which required coating with lead chloride to prevent low-angle total reflection from the vanes. Sample-to-detector distances of up to 49 cm are obtainable. Both photographic and counter detection are used.

Scattering patterns obtained with the instrument on samples of rabbit reticulocyte ribosomes are interpreted to determine the radius of gyration of the particles of 105 A to 2 per cent and the molecular weight of 4.1×10^6 to about twenty per cent. No evidence of secondary scattering maxima was observed. The electron density of the sample is approximated by a Gaussian consistent with the data with a cutoff at 170 A, giving in connection with electron microscope data of Professor Hall a hydration of 2.7 g water per g ribosome.

TABLE OF CONTENTS

I. LOW-ANGLE X-RAY SCATTERING OF SMALL PARTICLES

Low-angle X-ray scattering is an important method for the determination of the size, shape, and structure of small particles in a size ranging from about twenty angstroms in diameter to several hundred, and even larger. This method has many uses in biology, chemistry, physics, and metallurgy, and their industrial applications.

The work to follow describes the construction of a point-focusing X-ray crystal monochromator for low-angle scattering work and its application in the study of several materials, particularly the determination of the size and shape of rabbit reticulocyte ribosomes. Thus the present discussion will be concerned almost exclusively with biological applications, although the methods used are of more general application.

A. BRIEF COMPARISON OF LOW-ANGLE SCATTERING WITH OTHER METHODS

Several physical methods, such as light scattering, viscosity measurement, and the use of the electron microscope and the ultracentrifuge are also used to determine densities, weights, sizes, and shapes of small particles. The more direct of these methods, light scattering and the electron microscope, have serious disadvantages compared with X-ray scattering. Light scattering uses waves of several thousand angstroms wavelength. This is much too large a probe for a particle of a few hundred angstroms diameter, and consequently little information on structure can be obtained by this method. Obtaining the size of the particle from light scattering requires knowledge of the index of refraction

and absorption coefficient of the material. X-rays of one or two angstroms wavelength are small enough to resolve the interior structure of the particle, and except for extreme cases the absorption coefficients are such that the absorption is negligible in one particle. The index of refraction is so close to one as to be negligible.

The electron microscope, which is used to study about the same size range as low-angle X-ray scattering, has the important advantage that sizes and shapes of individual particles may be seen directly on the resulting pictures. Especially for biological samples, however, the requirement of having the sample dry and in vacuo means that the material may be so denatured that the results cannot be trusted. The X-ray method allows study of the material in solution at a desired temperature, a situation closer to the normal environment of organic substances.

The accuracy of results from low-angle X-ray scattering measurements depends on the accuracy of the measured intensity, the angle of scattering, the geometry of the instrument, and the wavelength of the radiation used. Except for the intensity, which depends on the particular experiment, these quantities may be measured precisely, and thus the X-ray method is of superior accuracy. The scattered intensity actually observed is caused directly by spatial variations in electron density in the sample particle and its surrounding medium. Thus if the intensity curve can be interpreted, it gives direct information about the size and shape of the sample material. This interpretation may be difficult, as will be discussed later. In any study, of course, information from all available methods is to be desired, that from low-angle scattering being

an important but not exclusive contribution.

B. GENERAL INTERPRETATION OF SCATTERING PATTERNS

Many authors have considered the problem of the interpretation of low-angle X-ray scattering patterns. The discussion here follows the treatment of Guinier and Fournet (1). Difficulty in interpretation arises from several causes. First, there is difficulty in interpreting the pattern of a single particle, particularly if the actual pattern observed is the averaging of this pattern over all orientations of the particle. Second, the pattern may be complicated by nonuniformities of size and shape among the particles and by aggregation and interparticle interferences. Third, organic samples have very low scattering intensities for X-rays of the wavelengths used, amounting even in favorable cases to only about 10^{-5} of the intensity of the incident beam. Large slits and apertures may be required to observe this intensity, and this requires slit corrections to be applied to the resulting patterns. These corrections may be difficult, particularly in the case where a circularly symmetric pattern must be scanned with a long narrow slit. A fourth difficulty arises when an already scattered ray is scattered again in the sample. This multiple scattering is negligible for low scattering cross sections dealt with here, and will not be discussed further. A fifth problem arises if the X-ray beam is poorly monochromatized, but as the studies to be discussed were done with a crystal monochromator which affords far better monochromatization than needed this problem need not be extensively discussed. The other problems will be discussed briefly here because they control the work to

be discussed later.

1. Scattering from a Single Particle

Scattering from a single particle is described by means of the structure factor, $F(\underline{h})$, for the particle such that:

$$I(\underline{h}) = I_e(\underline{h})F^2(\underline{h}) \qquad (1)$$

$\underline{h}$ is a vector commonly used to measure the deviation of the scattered wave. $\underline{h}$ will be precisely defined below. Letters with a bar underneath represent vectors whose absolute values are represented by the same letter without the bar. We will use the following symbols:

λ	the wavelength of the X-ray radiation
$\underline{s}_o$	a unit vector in the direction of the incident unscattered beam of X-rays
$\underline{s}$	a unit vector in the direction of the scattered wave
$\underline{r}$	a position vector from the origin of a coordinate system fixed in the particle
p	the distance in centimeters from the particle to the scanning slits
v	indication of integration over the volume of the particle
ϕ	the scattering angle
$I(\underline{h})$	the scattered intensity
$I_e(\underline{h})$	the intensity that would be scattered by a single electron
I_o	the intensity of the radiation incident on the particle
$\rho(\underline{r})$	the number of electrons per unit volume at a point in the sample

With these definitions, the following relations hold:

$$\underline{h} = \frac{2\pi}{\lambda}(\underline{s} - \underline{s}_o) \tag{2}$$

$$h = \frac{4\pi \sin(\phi/2)}{\lambda} = \frac{2\pi\phi}{\lambda} \tag{3}$$

$$F(\underline{h}) = \int_V \rho(\underline{r}) \exp(-i(\underline{r}\cdot\underline{h}))\, d\underline{r} \tag{4}$$

$$I_e(\phi) = 7.90 \times 10^{-26} I_o p^{-2}(1+\cos\phi)/2 \tag{5}$$

$$= 7.90 \times 10^{-26} I_o/p^2 \tag{6}$$

We can use the small angle approximations for the sine and cosine of the scattering angle. I_e is obtained from the expression for the classical coherent Thomson scattering. The formulas assume, of course, negligible absorption in the particle. Note that the structure factor is essentially the Fourier transform of the electron density distribution.

In most samples the particles are not oriented, and therefore the single particle scattering intensity that is relevant is the following:

$$\overline{I(\underline{h})} = I_e(\underline{h})\overline{F^2(\underline{h})} \tag{7}$$

where the bar over a function indicates the average of the function over all possible orientations of the sample particle. In this case Fourier inversion to obtain the density is impossible for an arbitrary particle. For a spherically symmetric particle however, the equation for $F(\underline{h})$ reduces to:

$$hF(h) = \int 4\pi r\rho(r) \sin(hr)\, dr \tag{8}$$

For particles suspended in a medium the effective electron density is the excess (or defect) of the electron density of the particle over the electron density of the medium.

2. Nonuniformities and Interparticle Interferences

In samples of appreciable concentration there will be scattering from the density variations between the particles as well as within them. For this reason it is generally necessary to extrapolate scattering curves to zero concentration. If the particles are identical this extrapolated scattering curve will be the curve for a single particle multiplied by the number of particles scattering. If the particles are not identical, interpretation is complicated. In biological samples aggregation of particles is common, and this may make it impossible to interpret the pattern.

3. Slit Corrections

Consider a circularly symmetric scattering pattern. Let us take the relatively narrow central beam to be centered at the origin of a Cartesian coordinate system with x and y measured in units of h. Let the pattern be scanned by moving a rectangular slit along the x axis so that center of the rectangle is on the axis and the sides of the rectangle remain parallel to the coordinate axes. The total breadth of the slit in the x direction is termed the slit width and the total breadth in the y direction is termed the slit height (see fig. 1a). Similarly are defined height and width for the central unscattered beam, although the beam is in general not of rectangular cross section. We define the following functions:

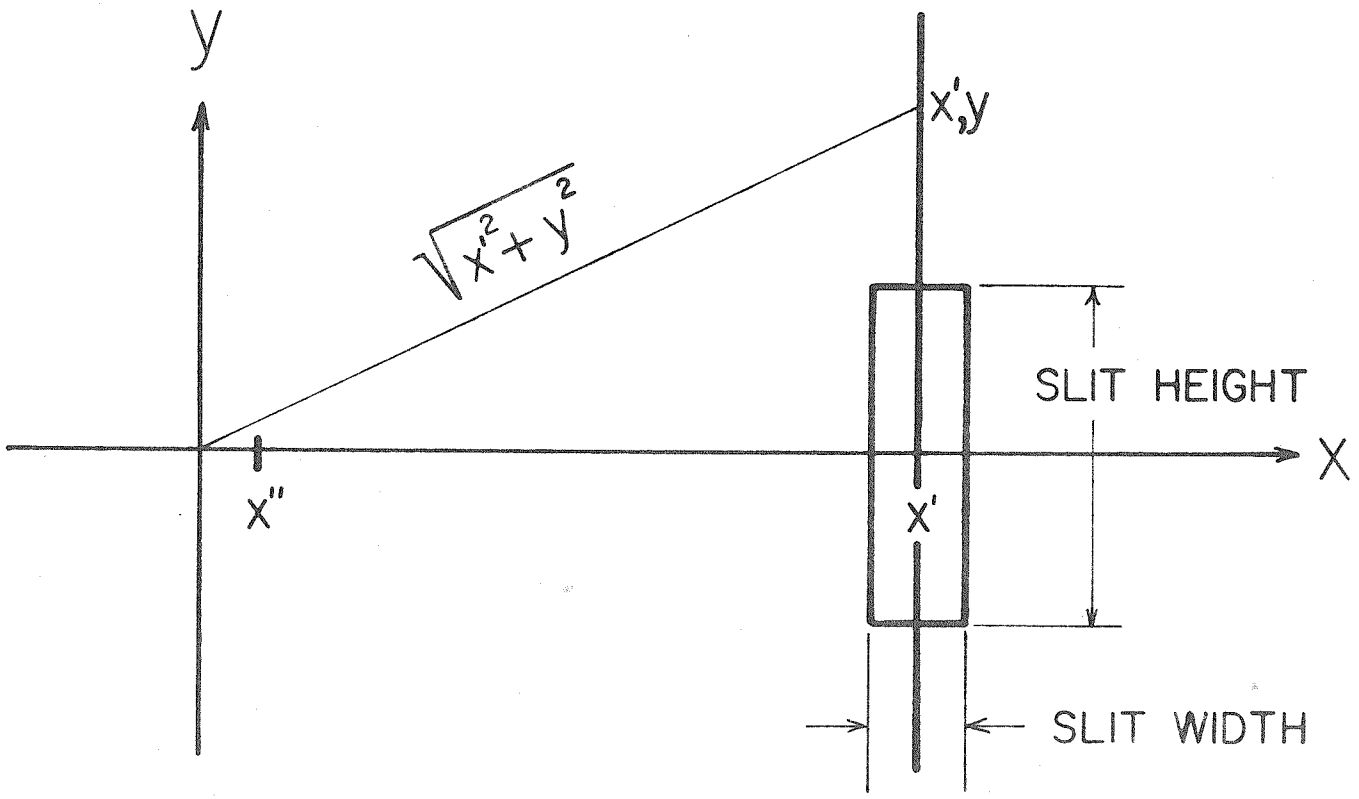

Fig. 1. Geometry of slit correction. The slit is centered at the point x'. Both the pattern and the central unscattered beam are centered at the origin of the coordinates. The vertical line $x = x'$ represents a slit of infinite height and negligible width. The variable x'' runs over the unscattered central beam.

$J_o(x)$ the intensity (power per unit of h) observed by scanning the pattern with a slit of infinite height

$J(x)$ the intensity (power per unit of h) observed by scanning the pattern with a slit of infinite height and negligible width under the conditions that the central beam also be of negligible width. If the central beam is of finite height, then this height is also negligible compared to the slit height.

$j(x)$ the intensity (power per unit of h) observed by a slit of infinite height traversing the central beam, with the condition that $j(x)$ is normalized so that the integral of $j(x)$ over the whole central beam is equal to one

$I(x)$ the intensity (power per square unit of h) observed if both the beam and the scanning slit are of negligible height and width

Now if the point $x = x'$ is the position of the slit at which the intensity is being measured, and the point $x = x''$ runs over the central beam, then it can be shown:

$$J_o(x') = \int_{x''=-\infty}^{x''=+\infty} j(x'')J(x'-x'')\,dx'' \qquad (9)$$

This may be solved for $J(x')$ by the use of Fourier transforms. This solution corrects for the slit and beam width. (2) The $J(x)$ so obtained is the scattering pattern for a beam of negligible height and width and a slit of infinite height and of negligible width.

The integral equation for the slit height correction may also be easily written down. If the intensity measurement is being taken at a point $x = x'$ then:

$$J(x') = \int_{y=-\infty}^{y=+\infty} I\left((x'^2+y'^2)^{1/2}\right) dy \qquad (10)$$

Solution of this equation for I(x) corresponds to the slit height correction. This is usually very difficult. A graphical method of solution has been devised which requires the derivative of the scattering curve. (3) The derivative is difficult to obtain precisely because of statistical uncertainties in the data. Of course if the pattern is not circularly symmetric but is instead composed of spots or lobes, the correction is impractical.

C. SPECIAL INTERPRETATION OF SCATTERING PATTERNS

Several methods have been devised for extracting information about the scattering particle from low-angle X-ray diffraction patterns.

1. Scattering from a Sphere of Uniform Density

Scattering from a sphere of uniform density exhibits secondary maxima and minima. The positions of these minima, which are nearly independent of the concentration, may be used to recognize such particles and to measure their common radius. Such maxima and minima were observed in scattering patterns of latex spheres by Danielson, Shenfil and DuMond, and checked with electron microscope studies which showed the particles to be spheres with radii varying by less than 10 per cent. (4) The method was used successfully by the Wisconsin group (5, 6) in measuring the sizes of spherical viruses.

2. Determination of the Radius of Gyration

It has been shown by Guinier (7) that as h approaches zero, $\overline{F^2(h)}$ for any particle approaches:

$$F^2(h) = n^2 \exp\left(-\frac{h^2 R_o^2}{3}\right) \qquad (11)$$

where

$$R_o^2 = \frac{\int_v r^2 \rho(\underset{\sim}{r})\, d\underset{\sim}{r}}{n} \qquad (12)$$

Here $\underset{\sim}{r}$ is a vector from the electronic center of mass of the particle, and n is the number of electrons per particle. R_o is termed the radius of gyration of the electronic charge of the particle about its electronic center of mass. As Guinier has shown, this radius of gyration may be determined from the slope of the scattering curve if the logarithm of the intensity is plotted against h^2. This slope is independent of the slit height correction as may be proved by letting $I(h)$ be a Gaussian in equation 10. This is therefore a readily measurable parameter of the scattering particle.

3. Determination of Mass of the Particle

As h approaches zero the scattered intensity of a sample containing N identical particles irradiated by the incident beam approaches:

$$I_o(0) = I_e(0) N n^2 \qquad (13)$$

The total number of electrons in the mass of the sample active in scattering is given by Nn. This can be determined from the chemical composition of the sample material. Thus equation 13 may be solved for n, which in turn gives the mass and other parameters of the particle. (8)

These formulas will be used in the interpretation of data taken in

Parts III and IV. It should be noted that the first method requires uniform density of the sample and may not hold if the particle diverges too greatly from this condition. The second and third methods require only that a sufficient percentage of the particles be identical. The first two depend only on the form of the scattering curve, while the last depends on the absolute intensity and requires measurement of the unscattered central beam, which is perhaps 10^5 times as intense as the scattering curve. The first method is not appreciably affected by interparticle interferences, and can therefore be applied in concentrated solutions, while the other two require extrapolation to zero concentration, and to zero angle as well.

II. INSTRUMENTATION

A. CONSTRUCTION OF A PHOTOGRAPHIC RECORDING POINT-FOCUSING X-RAY MONOCHROMATOR FOR USE IN LOW-ANGLE X-RAY SCATTERING STUDIES

A point focusing X-ray monochromator was constructed and used for obtaining low-angle X-ray scattering patterns. This instrument uses an X-ray focusing geometry developed independently by Despujols (9) and by Berreman (10) and applied to elastically bent quartz crystals by Berreman, who used this method to study low-angle scattering patterns. (11)

1. Focusing Geometry of the Instrument

The reflecting quartz crystal of this instrument is cut and bent in such a way that X-rays from a point source are to a very good approximation focused to a point, after being selectively reflected by Bragg reflection at the surface of the crystal. The process of cutting and bending a thin quartz crystal lamina to achieve this is illustrated in fig. 2. The basis of this procedure may be most easily explained by referring to fig. 3, which shows the focal circle of a curved-crystal X-ray spectrometer, as devised by DuMond. (12) The point P_1 is the position of a line source of X-rays perpendicular to the plane of the diagram. Similarly, P_2 is the position of a line image formed by a monochromatic beam of X-rays from P_1 after being reflected at the Bragg angle, θ, from a crystal centered at O. The condition for exact line to line focusing, as shown by DuMond, is that the crystal boundary surface be bent to a cylindrical radius, $R_1/2$, while the crystal planes are bent to a concentric cylinder

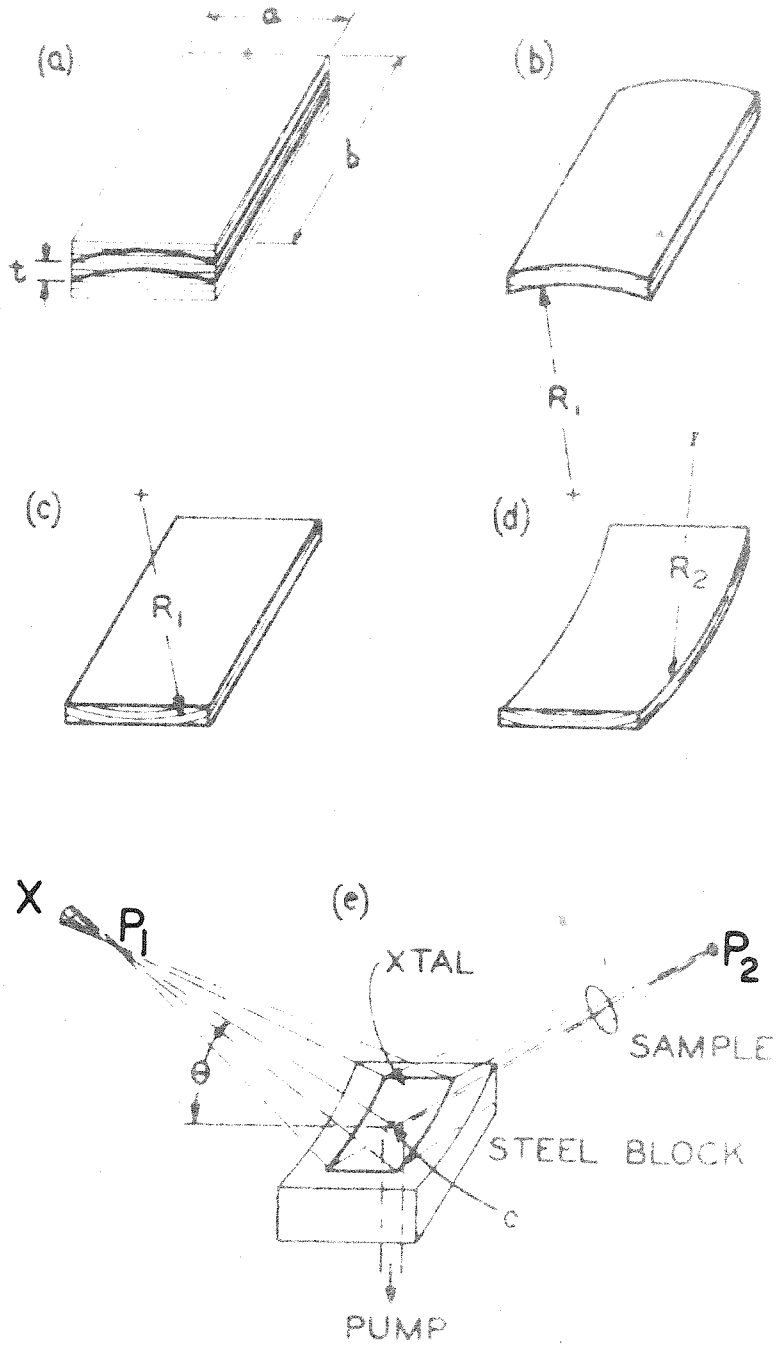

Fig. 2. Process of making a single-crystal point-focusing X-ray monochromator. a and b **are 2 1/2 and 2 3/8 in. respectively. Other dimensions are listed on page 18. Diagram used through courtesy of D. W. Berreman.**

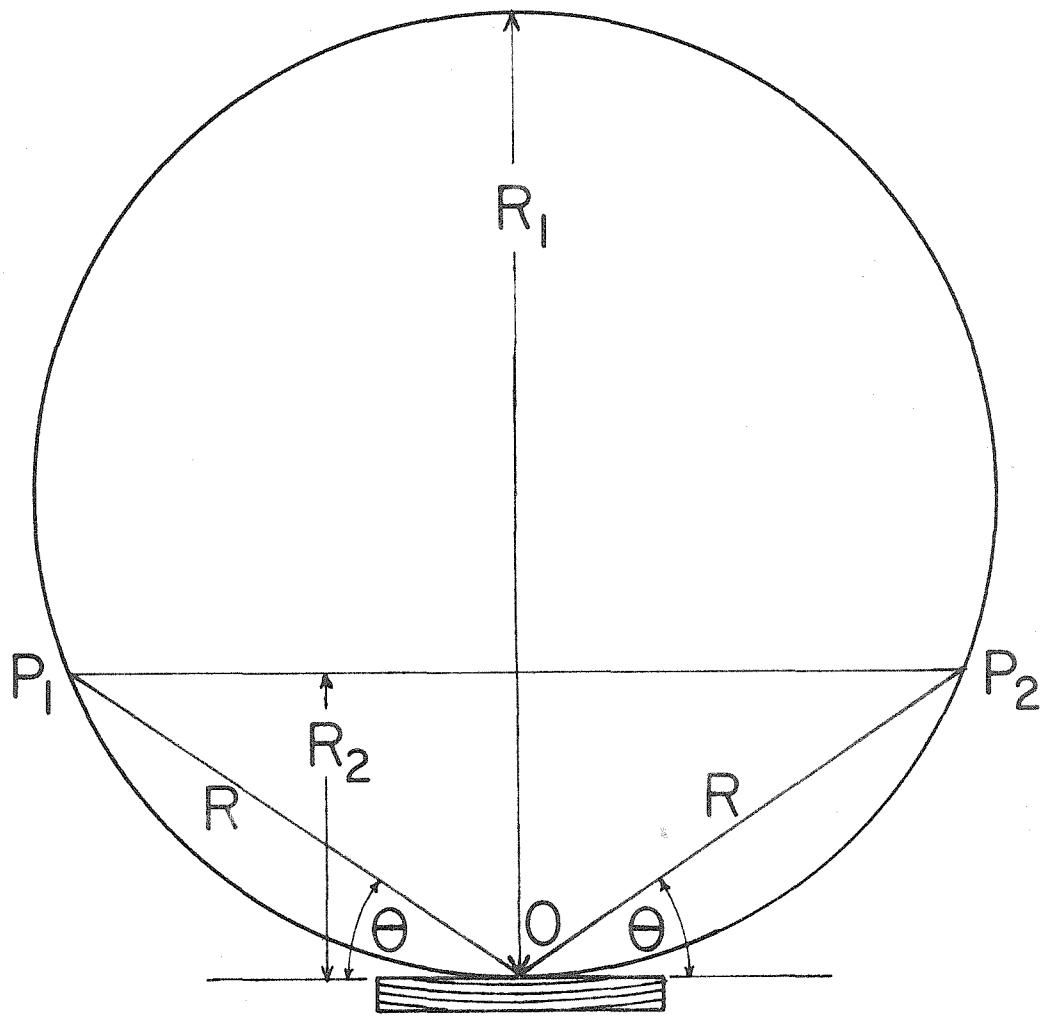

Fig. 3. Geometry of point-focusing X-ray monochromator. P_1 and P_2 are the source and image points respectively. θ is the Bragg angle. R_1, the diameter of the circle pictured, is the radius to which the crystal planes of the crystal surface at O are curved.

with radius R_1 for that plane which is tangent to the boundary surface. This requires that the crystal lamina before bending be cut in the unstressed state to a concave cylindrical surface of radius R_1. A successful approximation to the DuMond spectrometer may be obtained by bending an initially flat crystal lamina to the radius R_1 so that the crystal planes are at the right curvature, i. e., have the right orientation, but the boundary surface of the crystal is not in the right position except at the point of tangency of the reflecting surface with the focal cylinder. (13)

A further approximation was introduced by Berreman: He reasoned that if the error in position of the reflecting surface just alluded to could be tolerated, then an error of double this amount might also be acceptable. The crystal in its unstressed state was cut to form a thin cylindrical lamina of radius R_1 as shown in (a) and (b) of fig. 2, and then the crystal was flattened, as shown in (c) of that figure. In this state the surface of the crystal was flat while the crystal planes were bent to the correct radius to give approximate focusing of a focal cylinder of radius $R_1/2$. From this flat condition the crystal lamina could next be bent to the radius R_2, the bending in this instance, however, being in a direction at right angles to the curvature of the original cylindrically cut lamina, with the result as illustrated at (d) in fig. 2. Now the lines P_1 and P_2 of fig. 3 may be considered as points, and the figure has an axis of cylindrical symmetry through these two points. Radiation from P_1 would be focused at P_2 after reflection from the crystal. Note that this result has been achieved with minimum distortion of the crystal since only cylindrical bending has been applied. It can readily be shown that in

order to focus radiation of a wavelength λ such that the Bragg planes of the crystal will reflect it selectively at the Bragg angle θ (related to λ by the Bragg relation, $n\lambda = 2d \sin \theta$) it is necessary that R_1 and R_2, the two radii of curvature in this double focusing arrangement, shall satisfy the relation, $R_2/R_1 = \sin^2 \theta$. Thus, with a fixed ratio of radii, one and only one wavelength can be selectively point focused.

The point P_1 corresponds in the completed instrument to an aperture through which X-rays pass, and which serves as the object point for this X-ray optical system. This aperture will be referred to as "the aperture at the X-ray." The point P_2 corresponds to the point at which X-rays from the object point P_1 converge after reflection from the crystal. This point will be referred to as the "X-ray focal spot," or "X-ray focus," or simply as the "focal spot," or "focus."

The accuracy of the approximation in this focusing geometry as well as the effect of finite source size and the extension of this method to more general geometries are extensively discussed by Berreman. (14)

The great advantage of this type of instrument is the attaining of a high X-ray intensity at a point focus, while at the same time giving a monochromatic beam. Berreman calculated an advantage in intensity of a factor of fifty over the most ideal instrument of comparable resolution using pinholes to collimate a direct X-ray beam, and a factor of about two hundred over a practical device with monochromatization by balanced filters. Of course this disadvantage may be more than overcome by using slit collimation of a direct X-ray beam from a rotating anode X-ray tube, as Beeman has done (15), but then much information may be lost by the

smearing effect of the slits, and difficult slit height corrections will be necessary.

2. Specifications for the New Instrument

It was decided to build a monochromator of the above design for use in low-angle X-ray scattering experiments that would have a higher intensity beam than the prototype which Berreman had constructed. At the same time it was desired to simplify the lining up procedures and to improve upon another feature of Berreman's prototype which we shall now explain. Berreman had found that a converging vane collimator is necessary in order to suppress the halo appearing around the central beam of the monochromator. This halo, he showed, results from diffuse scattering by the bent crystal. Although this halo is very faint in relation to the primary point focus, it may, for weakly scattering specimens, compete very objectionably with the low-angle scattering pattern to be studied. It was decided to build a converging vane collimator of increased angular resolution.

At Dr. Berreman's suggestion, the 023 planes of quartz were chosen for the planes of reflection since they have a reasonably large Bragg angle, a high reflection coefficient (16), and are near the standard BT cut of the quartz crystal. The instrument was designed to use copper $K\alpha_1$ line radiation. Since this wavelength is greatly absorbed by air, the instrument was designed so that the beam would travel through an atmosphere of helium. The principle dimensions of the instrument and some other information are as follows:

Wavelength $CuK\alpha_1$ Line	λ	1.540 A
Various Radii	R	36.57 in.
	R_1	62.25 in.
	R_2	20.492 in.
Bragg Angle	θ	$34^{\circ}5'$
Sine of Bragg Angle	$\sin\theta$	0.56040
Crystal Thickness		0.015 in.
Other Crystal Dimensions		2-3/8 x 2-1/2 in.
Bragg Planes		023

3. General Layout of the Instrument

The instrument constructed is shown in fig. 4. The points P_1, O and P_2 correspond to the aperture at the X-ray source, the center of the reflecting surface of the crystal, and the X-ray point focus respectively. These points correspond to the points labeled in the same way on fig. 3. The X-ray tube, in these experiments a General Electric CA-7 copper target diffraction tube, is placed with one of its beryllium windows against the aperture at P_1. In these experiments the particular window and the position of the X-ray tube were chosen so that the 0.8 by 15 mm source on the X-ray tube target would appear approximately as a square from the aperture of the instrument in order to obtain as intense a beam as possible. The position of the X-ray tube can be adjusted in two mutually perpendicular directions normal to the axis O-P_1 and can also be adjusted back from P_1 along the same axis. The X-ray tube and its adjustments and shielding rest upon a framework of steel I-beams, to which are attached the four hard rubber wheels upon which the whole

instrument rests. On this frame also, held by a framework of angle irons welded to the I-beams, rests the main body of the instrument. This is comprised of a large steel drum, to which are attached the two steel tubes as shown in the figure.

The aperture at P_1 is adjustable in two orthogonal directions on the end plate of tube 2, the smaller of the two tubes shown in fig. 4. Also, the very small tube in which the aperture itself is fixed may be screwed in and out along the axis $O\text{-}P_1$. All of these adjustments are sealed by O-rings, and the aperture itself is sealed by a film of aluminum coated Mylar so that the instrument is light tight and gas tight at this end, and in fact generally, except for the provision for circulation of helium and coolant for the sample.

Both the sample holder and the film holder run along a track comprised of two 3/4 in. drill rods mounted vertically in the large tube on either side of the beam. Thus, both sample holder and film holder may be positioned vertically. The film holder holds a piece of photographic X-ray film at the focus P_2. A small lead button held by a tungsten wire prevents the central X-ray beam from striking the film and thus prevents halation. The shadow of the tungsten wire is arranged to fall in the area darkened by that azimuth of the halo radiation which is not stopped by the collimator so that said shadow does not further mar the pattern. The lead button may be pushed to one side momentarily so that the center of the pattern may be marked by the beam.

Tube 1 is open to allow access to the film holder and the sample holder as shown in fig. 4. This tube is sealed off during operation of the instrument by means of a cylindrical sleeve which fits over tube 1, closing

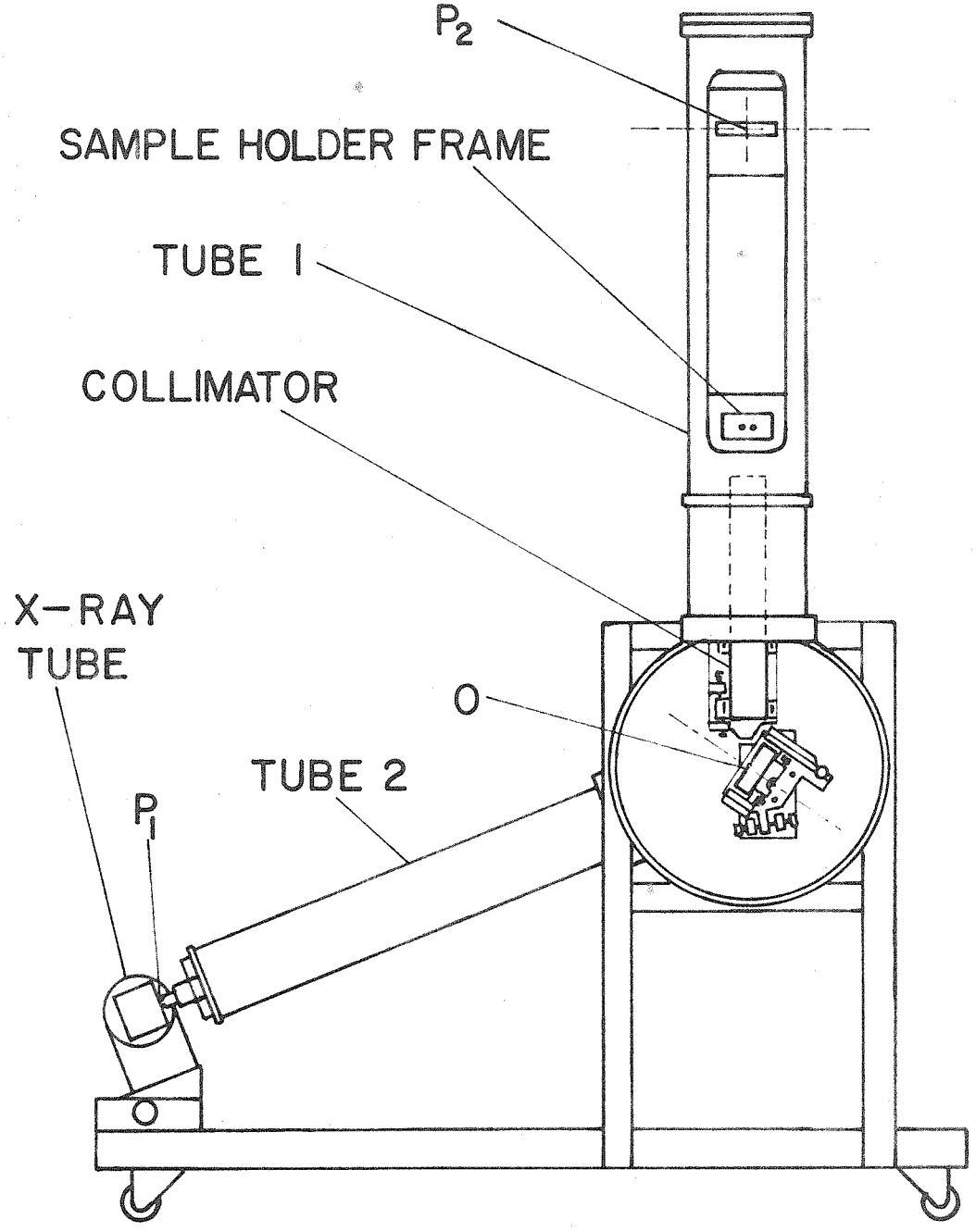

Fig. 4. Photographic-recording point-focusing X-ray monochromator for the study of low-angle X-ray scattering patterns. P_1 locates the aperture at the X-ray tube and P_2 indicates the point focus. The reflecting surface of the doubly-bent quartz crystal is centered at O.

off the opening. This sleeve is sealed at each end by means of O-rings around tube 1 above and below the opening, which seal against the inner surface of the sleeve. The large drum is also provided with a cover to seal it shut during operation of the instrument.

4. Crystal and Crystal Mounting

A block of quartz, 2-3/8 by 2-1/2 by 3/8 in. was obtained from Monitor Products Company of South Pasadena, California. The large faces of this crystal were parallel to the 023 planes of the quartz as checked by an X-ray goniometer. Two crystal laminae of thickness 0.015 in. were cut from this quartz by the Penn Optical and Instrument Company of Costa Mesa, California. The crystal laminae were ground and polished by this company to a cylindrical radius of 65.25 in. One of the two crystals was found to have a long scratch on it, and it was decided to try to bend this crystal first.

The crystal was etched for 23 minutes in 51 per cent hydrofluoric acid, and then the edges of the crystal were etched for another four minutes each. The purpose of the etching is to dull the sharp edges of any cracks in the crystal and also to relieve any strains that might be caused by small particles of quartz being wedged into such cracks during the grinding and polishing operations. The crystal was successfully bent and was used for the experiments described herein.

The block to whose precision cylindrically profiled surface the crystal is attached, and which thus imparts the correct curvature to the lamina, was constructed of AISI type 420 steel with the following specifications:

Chromium	12-14%
Carbon	0.25-0.35%
Manganese	less than 1%
Silicon	less than 1%

This is a special stainless steel chosen for its excellent stability and because it matches as closely as possible the thermal expansion coefficient of quartz. Two blocks were machined to the desired size and then heat treated to the following specifications:

Heat to 950°C and quench in oil (such as No. 20 engine oil).

Draw at 800°C to a shore of 32.

The crystal block was then ground and lapped to a concave cylindrical surface of radius 20.492 in. The grinding was achieved on a surface grinder by means of a special linkage in the manner described by DuMond. (17)

The crystal was sealed to the block by the vacuum method described by Berreman. After the surface was cleaned and delinted as well as possible the crystal was placed on the block in the proper orientation. At this point a vacuum pump was turned on which connected to a small vacuum chamber sealed onto the back of the crystal block. This communicated with the space between the crystal and the concave curved surface of the crystal block by means of a hole through the center of the crystal block, as indicated at (c in fig. 2. At the time when this pumping began to evacuate the air between the crystal and the block, the edges of the crystal were painted with hot beeswax and the crystal was pressed down onto the block. To ensure a good seal the beeswax had to be pressed down with the fingers. When the small vacuum chamber on the crystal

block is sealed off the crystal remains without appreciable change for months if the seal is good enough; in practice provision was made for pumping on the crystal without opening the instrument or interrupting a run so that a seal which is good for a week or so is adequate. If necessary the pump can be kept on during an entire run.

The adjustment mechanism for the crystal is illustrated in figs. 14 and 15 in the Appendix pages 78 and 79 . The assembly provides for rotation of the crystal and block around three perpendicular axes in space which intersect in a stationary point. This point is designed to coincide with the center of the reflecting surface of the crystal, the point corresponding to the point O in the earlier diagrams. This point lies on the axis of symmetry of the large drum. This axis is perpendicular to the machined inside surface of the base plate of said drum. The crystal adjustment assembly is fixed to this base plate. Rotation of the crystal block about this axis which is horizontal in the actual instrument, corresponds to a change in the Bragg incidence angle, and is effected by the double screw and spring adjustment at A. A similar adjustment at B, and another at C complete the adjustment knobs for the crystal. The adjustment at C rotates the crystal about a line perpendicular to the surface of the crystal through its center. The adjustment at B rotates the crystal block together with the mechanism at C about the axis bb' parallel to the base plate of the large drum. This last adjustment aids in putting the focal spot in the right position on the photographic film.

5. Collimator

The collimator is needed to prevent a halo of radiation around the central spot from obscuring the radiation of the scattering patterns to be studied. Berreman has shown that this halo results from radiation diffusely scattered by the crystal in the neighborhood of the Bragg angle (11) and is extremely weak compared to the central focus, but, unfortunately, can compete objectionably in intensity with the diffraction patterns from the organic molecules which are to be studied. The collimator is located between the crystal and the sample to be studied as indicated in fig. 4. It consists of an array of converging vanes which are parallel to the rays of the converging beam from the crystal and also converge toward the X-ray focal spot, P_2. The resolution of this converging vane collimator does not affect the resolution of the scattering pattern--that is determined by the accuracy with which the crystal and the crystal block are ground. The collimator determines how much of the X-ray film is free from halo; i.e., how close to the unscattered central beam it is possible to take scattering data. Since some of the methods of interpretation of the scattering patterns require extrapolation of the curve to zero angle, it is necessary to have the resolution of the collimator as sharp as possible, especially for the larger particles, whose scattering patterns will be concentrately closely about zero angle.

The resolution of the collimator may be increased by increasing the number and decreasing the separation of the vanes, but, assuming that they are already as thin as practical, this means that more of the beam will be absorbed by the vanes. In the present instrument the number of

vanes was chosen by letting the separation of the vanes at the narrow end of the collimator be equal to the thickness of the vanes. This means that half the intensity will be absorbed from the beam by the collimator. Under this condition, the optimum length of the collimator may be determined by the calculation to follow (see fig. 5).

In this calculation angles are small enough so that they differ insignificantly from their sines. We define the following symbols:

t — the thickness of the collimator vanes and also the distance between them at the narrow end of the collimator

L — the length of the collimator

S — the distance from the narrow end of the collimator to the X-ray focus, P_2, and thus also the maximum sample-to-focus distance.

C — the sum of S and L, or in other words the distance from the broad end of the collimator to the X-ray focus

D — the width on a film at the X-ray focus of the region covered by that part of the halo not blocked by the collimator

d — a Bragg spacing in the sample

It may be easily shown that:

$$t = \frac{DL}{2S + 3L} \tag{14}$$

From Bragg's law it may be shown that for a spacing, d, whose scattered line falls just at the edge of the strip of width D on the film irradiated by the halo, and with sample-to-film distance S:

$$d = \frac{2S\lambda}{D} \tag{15}$$

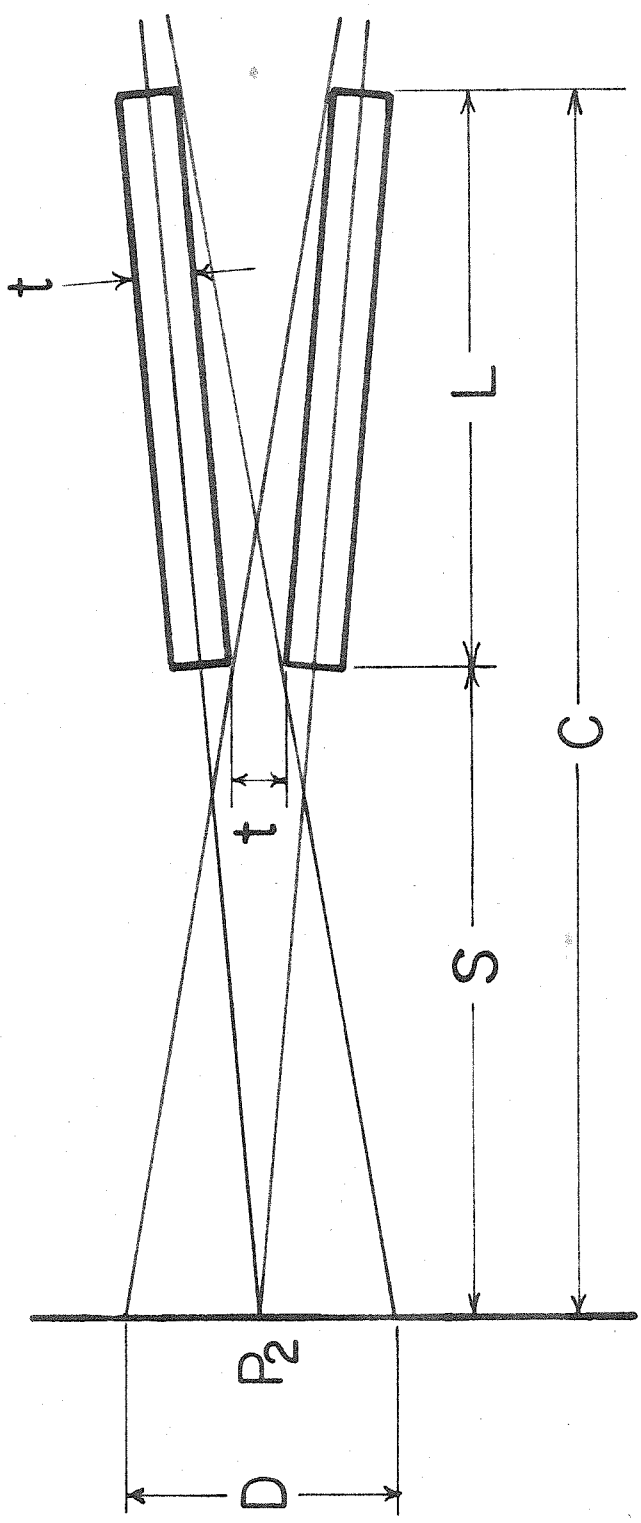

Fig. 5. Geometry of collimator calculation. The collimator is represented by two vanes of approximate length L and width t.

Eliminating D from these two equations, and using C to eliminate S:

$$d = \frac{2\lambda C(1-L/C)}{t(1+L/C)} \tag{16}$$

We are interested in values of L corresponding to maximum values of d, for given values of t and C. Setting the derivative of d with respect to L equal to zero we obtain:

$$\frac{dd}{dL} = \frac{-2\lambda(L^2+2LC-C^2)}{t(L+C)^2} = 0 \tag{17}$$

Whence, taking the positive root:

$$L = -C+C(2)^{1/2} = 0.414C \tag{18}$$

C is R diminished by 2.5 in. to allow for clearance between the crystal assembly and the collimator. This results in a value of L of about 13.75 in., which was chosen for this collimator. The vanes are made of tin plate about 0.010 to 0.011 in. thick. They are held in place by converging slots milled in the metal pieces which constitute two opposite walls of the collimator box. (See fig. 16 in the Appendix, page 80 for the completed collimator.) With this value of t one obtains about 1800 A for d. With the collimator after final correction for reflection as described below, d should be of the order of 600 A.

Tin plate was chosen for the vanes because it was readily available in thin flat sheets and was of higher atomic number than copper and thus would have a relatively high ratio of absorption to scattering (per atom) for copper Kα X rays. The collimator is provided with two adjustments. The first moves the collimator along the beam so that its focus may be

made to coincide with that of the crystal. The second rotates the collimator in the beam so that the vanes may be aligned parallel to the X-rays.

6. Avoiding Reflection from the Collimator Vanes

The greatest problem in the construction of a practical collimator proved to be the problem of stopping the radiation which was reflected from the collimator vanes at grazing incidence from striking the film. As can be seen from fig. 19 in the Appendix, page 83 , even short exposures are affected by this reflection which is much more intense than the halo that the collimator is designed to reduce. Berreman had used a collimator using lead plates which did not give appreciable trouble in this regard. The collimator described here is of greater resolving power and needs thinner vanes; thus lead vanes seem out of the question.

A device was built to allow testing of various surfaces to find one that would have low enough reflection. It was discovered that the material used for the surface had little effect on the reflection. Even lead surfaces when smooth and not too heavily covered with oxide reflected almost as well as other surfaces. This is to be expected, as, qualitatively speaking, the curves of reflection coefficient versus angle of grazing incidence for various metals are about the same. The nature of the surface was the most important factor; shiny surfaces in general had high X-ray reflections, while surfaces that appeared rough to the eye had the best characteristics.

After several attempts to solve the reflection problem with deposited coatings and other methods, the problem was finally solved by the

precipitation from aqueous solution of lead (plumbous) chloride onto the collimator vanes. The vanes are put in a bath consisting of a warm saturated solution of the lead chloride, which is then allowed to cool slowly. This allows fine crystals of the salt to grow on the surface of the vanes. If the lead chloride is deposited too fast, the crystals will not adhere, but if the solution cools slowly the crystals become very firmly attached, so that even if an attempt is made to rub them off after the vanes have dried a very thin coating of the crystals will still remain. This bonding may be affected by the fact that at the same time tin is replacing the lead in solution and lead is slowly being deposited on the surface of the vanes. The resulting surface has excellent non-reflection properties, as may be seen by comparing the short exposure of fig. 19 in the Appendix, page 83 with the longer exposures of the albumin pictures in fig. 22 in the Appendix, page 86 . The latter figure also shows where the halo comes through between the collimator vanes and marks a strip across the film. One disadvantage of this process was that the deposition so thickened the vanes that they could not all be used in the collimator without absorbing nearly all of the beam. In the following experiments the collimator was used with only 38 of its 75 vanes in position and in this condition absorbed about forty per cent of the beam.

It is believed that the increased surface roughness is principally the cause of the decreased reflectivity of the collimator vanes, but another factor may help. The X-rays on striking the lead chloride crystals should be scattered into diffraction rings as in a powder camera. Most of these rings would be at too high an angle either to get out of the collimator or

to interfere with the small angle part of the pattern. This would leave a relatively clean central beam.

7. Sample Holder

Organic samples must often be kept in aqueous solution in the instrument for hours or days without evaporation of the solution and without degradation or other changes in the sample. If the sample is in helium atmosphere, it is important that the helium not diffuse into the sample frame and distort it. The material which contains the sample and through which the X-ray beam passes must absorb as little of the beam as possible and contribute as little as possible to the small-angle scattering.

The sample cell is ideally a rectangular lamina of some inert solid substance one millimeter thick with a rectangular window cut through it large enough so that the X-ray beam may pass through it without touching the edges of the window. A thin film is required on each side of the lamina to hold the sample in this thin cell formed by the lamina window. It is well known that the maximum scattering from such a laminar sample is obtained when the sample is of sufficient thickness to absorb 1/e of the incident beam, assuming negligible multiple scattering. For water, this thickness is approximately one millimeter, and accordingly, this thickness was chosen for the sample thickness. For more concentrated organic solutions, and at certain ionic strengths, this dimension is not strictly accurate; fortunately, this dimension is not critical, and samples give very nearly the same scattering for comparatively wide variations from this ideal thickness. The 1/e absorption applies only to the absorption in the substrate containing the material whose scattering curve is required; further absorption in the films, or in the

helium path, does not change the condition.

Teflon and Marlex have been used to make the sample frame because they are chemically inert to our sample materials. Marlex is particularly good because of its rigidity; however, care must be taken to keep it out of the beam as it has appreciable small-angle scattering. The thin films are attached and sealed to the frame with Dow Corning silicone vacuum grease, the use of which has proved entirely satisfactory in containing the specimen and affords easy changing of sample materials.

Since the sample frame is immersed in an atmosphere of helium, it is important that neither helium, nor the water inside the frame, be able to diffuse through the thin film containing the sample. Containing the water, of course, is the easier of the two problems, although thin organic films, such as 0.0025 in. thick Mylar, allow the water to evaporate through the film. Mica and Parafilm have been used successfully, and undoubtedly other films would also perform satisfactorily. It would be possible to saturate the helium with water vapor before letting it into the apparatus, but then care would have to be taken to insure that the entire instrument was at the same temperature; otherwise condensation would occur on the sample holder, which is generally cooled. Keeping the helium from diffusing into the cell and forming bubbles which distend the sample proved to be impossible with the organic films available, and therefore mica was used for samples which had to be run in helium atmosphere.

Fig. 17 in the Appendix, page 81 , shows the Marlex sample

frame and the brass sample frame holder. One sample frame is shown installed in the sample frame holder and the other is shown leaning on the side of the holder with one of the Parafilm films partly pulled back.

The brass sample frame holder also serves as a cooling jacket to cool the sample. In the above mentioned figure two tubes are shown attached to the holder. These connect to a channel or tunnel wholly contained within the brass of the brass sample frame holder which goes around the holder to form a single cooling loop. This one loop will successfully cool the sample, but in practice several more loops of copper tubing were added in the instrument just above the sample frame holder to increase the speed at which the sample could be cooled. The coolant was pumped through the sample from a reservoir in a water cooler, which was held at about four degrees below zero centigrade by a thermostat comprising a Fenwal thermoswitch connected to relays which controlled the pump of the water cooler. A mixture of glycerine and water served as the coolant. Trials with a copper-constantan thermocouple junction in the middle of the sample frame indicated that with the reservoir at zero degrees centigrade the sample could be held under five degrees centigrade, adequate for the intended applications.

8. Search for a Suitable Sample Holder Film

Several difficulties arise in choosing a suitable film for containing the sample on the sides through which the X-ray beam passes. Some of these have already been discussed; others, the problems of absorption, scattering, and rigidity, will be discussed here. None of the materials yet used or tested can be considered even approximately ideal, but mica and Parafilm have been used successfully.

The first series of ribosome runs to be described used a sample holder frame of 1/32 in. thick Teflon and films of mica backed with 0.001 in. thick Nylon. Mica seemed the only answer as long as the sample had to be kept in a helium atmosphere. The Nylon film was also used, being placed next to the mica on the inside in order to keep the sample from coming in contact with the mica. It seemed certain that Nylon and Teflon would not interact chemically with the sample, but there was some doubt about the mica. Thin sheets of mica are relatively rigid, but even thin sheets have high X-ray absorption. The total thickness of mica had to be under 0.002 in. thick in order to get two thirds of the beam through the mica. Mica is brittle, especially in thin sheets, making it difficult to change samples without breaking the films. If the sheets are made much thinner than 0.001 in. thick each, they are too fragile to use.

In the second series of ribosome runs, Marlex 0.04 in. thick was used for the sample frame, and Parafilm 0.005 in. thick was used for the containing film. Parafilm is a film prepared from paraffin wax by adding a few percent of polyethylene. It has low absorption and low enough scattering in the region of interest, but it is flexible and easily distorted. Nevertheless, it could be made to lie sufficiently flat on the sample holder frame to maintain the shape and volume of the sample chamber, and had sufficient strength to allow emptying and refilling of the sample frame.

Approximate tests of several common plastic films were made to determine the absorption of X-rays of this wavelength. Parafilm, polyethylene, and Marlex showed outstandingly high transparency to X-rays.

All of these substances are chemically similar in consisting of long paraffin series type hydrocarbon chains, but they differ in the way these chains are connected. Marlex is a form of polyethylene in which there is much cross-linking of the chains so that it is particularly rigid. It was hoped that it could be used because of this property.

Low-angle scattering curves were taken of Parafilm, polyethylene, and Marlex. Of these three only the Parafilm had sufficiently low scattering in the low angle region to be used to contain the sample. Both the Marlex and the polyethylene showed an intense, broad maximum in the very region important for particles as large as ribosomes, the polyethylene maximum being much the broader of the two. Therefore they could not be used, despite their more attractive mechanical properties.

B. USE OF THE PHOTOGRAPHIC INSTRUMENT

1. Lining Up Procedure

To line up the instrument, the aperture at the X-ray end is approximately centered on the plate on which it slides. The crystal adjustments are also centered as closely as possible by eye. Then the X-ray tube is adjusted until radiation floods the crystal, as may be determined by a photographic film, a counter, or a fluorescent screen. Then, with a detector at the X-ray focus, the Bragg incidence angle adjustment of the crystal is changed until radiation is detected at this position. In the event this does not succeed, the detector may be placed closer to the crystal to start with. At this stage the collimator should not be in the beam unless it is known to be in correct adjustment. Once radiation

is detected at the X-ray focus, the location of the focus may be determined by photographic or other means. This focus, P_2, may be moved in the direction perpendicular to the plane of figs. 3 and 4 by using the the adjustment B on the crystal adjustment (see fig. 14 in the Appendix, page 78). The focus may be moved in the other direction perpendicular to the beam only by moving the aperture at the X-ray source an approximately equal distance along the plate. If the instrument is being lined up for the first time it will probably be necessary to repeat the above procedure for several distances of the aperture from the crystal in order to determine the value of R for which optical aberrations are a minimum so as to have the sharpest focus obtainable; otherwise the above procedure should suffice.

Once the focus is located, the moving of either the X-ray tube or the Bragg incidence angle adjustment on the crystal will not alter the position of the focal spot. Therefore both of these may be adjusted successively to obtain the maximum possible intensity in the beam. Care should be taken that the copper $K\alpha_1$ line is used and not the copper $K\alpha_2$ line, as the instrument will separate the two and can be aligned to use either. The $K\alpha_1$ is used because it is the more intense of the two.

Next, the collimator may be installed, and adjusted for maximum transmission.

2. Operation of the Instrument

The instrument was operated using a General Electric CA-7 water-cooled copper-target diffraction tube running at 45 kilovolts and 18 milliamperes. The X-ray path within the instrument was filled with

helium. With an aperture of 0.0225 in. diameter at P_1 a point focus at P_2 was obtained with a half width of about 0.025 in. in one direction and 0.015 in. in a perpendicular direction. The narrower half width is the width determined by the $K\alpha_1$ line resolution by the Bragg reflection. With the collimator in the instrument, central beam intensities up to about 10^9 counts per minute have been calculated from Geiger counter observations, without correcting for the efficiency of the counter. This would mean about 3×10^9 counts per minute for the central beam unobstructed by the collimator.

The reflected intensity of the crystal in this instrument was compared with that of Berreman's instrument using the 052 planes. Provision was made for mounting each of the crystals in the crystal position of the new instrument, and a narrow beam of X-rays about two mm square was allowed to fall on the crystals, each in turn. The maximum intensity obtainable on reflection from each, relative to the intensity of the incident beam, was measured. The 023 planes had a reflection coefficient greater than that of the 052 planes by a factor of 2.1 (see Table I). Berreman has measured the reflection coefficient of the 052 planes in order to compare it with his predicted values. (11) Using this measurement and his predictions together with the above comparison of the reflectivities, Table I may be compiled. The experimental values should be regarded as approximate. The third entry in the table differs from the second in that it does not include the increased reflection caused by X-rays striking planes in the crystal at slightly different angles as they penetrate deeper into the crystal. In Berreman's calcu-

lations this effect contributes more than the surface reflection. If we consider just the reflection from the surface, then the ratio of the intensities is closer to the measured value, although the actual intensities are even further from experiment. The major part of this discrepancy is undoubtedly caused by the fact that for the 023 planes the angular width of the reflected $K\alpha_1$ line is less than the 0.0225 in. diameter of the aperture at the X-ray. Thus much of the incident line radiation will be at the wrong angle for strong reflection. (11)

Table I

Crystal planes	052	023	ratio
Measured reflection coefficient	0.028	0.06	2.1
Calculated reflection coefficient	0.0167	0.077	4.2
Calculated, surface reflection only	0.0066	0.0182	2.76

3. Keratin Exposures

The results of runs on Keratin samples are shown in fig. 20 in the Appendix, page 84. The exposures were made with the X-ray running at 45 kilovolts and 18 milliamperes, which is also true for all the work reported here unless otherwise mentioned. The upper exposure was made at a sample-to-film distance of 12.5 cm. for 34.3 hours. The lower exposure was at a sample-to-film distance of 27 cm. in order to show an enlargement of the low-angle region, and was exposed for 100.3

hours. The keratin samples used in this experiment were parallel aligned strips of the white portions of the base of seagull feathers. In the more magnified keratin exposure the darkest, most obvious spots (partly smeared into a ring) correspond to a Bragg spacing in the sample of about 24 A. The large diffuse spots correspond to a spacing of about 34 A. The smallest ring visible corresponds to a spacing of about 50 A, and there is a clear indication of a pair of spots inside this ring corresponding to a spacing of about 75 A. The magnification of the pattern could be increased by almost a factor of two by increasing the sample-to-film distance to the maximum for the instrument of 48 cm.

These exposures show clearly some of the advantages and disadvantages of this type of instrument. Any attempt to observe this type of diffraction pattern with a line-focusing instrument would have resulted in grossly smearing the pattern, and losing too much information. The photographic method of detection is clearly advantageous here also, as the film takes data at all parts of the pattern at the same time; trying to run over this whole pattern area with a small window in front of a Geiger counter would be much less satisfactory. A further advantage is afforded by the excellent monochromatization of the instrument -- in conventional X-ray diffraction pictures using unmonochromatized radiation, the central part of the pattern is obscured by scattered bremsstrahlung. In these present exposures, the center is relatively clean.

Unfortunately, these pictures also expose one disadvantage of the instrument. In order to use the intensity afforded by this instrument, it is necessary to use a sample as broad as the beam at the same position. This means, with a sample thickness of about one millimeter, that the

least volume of the sample must be about 0.6 ml, or in the case of keratin discussed here, the sample must be from six to eight square centimeters in area. It is difficult to obtain sufficiently well aligned samples of keratin from seagull feathers even for very small samples, and nearly impossible for the broad samples needed here. This same requirement on the size of the sample also diminishes the usefulness of the instrument for such samples as single virus crystals, which are too small to intercept much of the radiation. Of course it is possible to restrict the beam to a narrow pencil, which could then be very accurately focused, and taking exposures for very long times, but this would be abandoning one of the chief advantages of this instrument, its high intensity.

4. Albumin Exposures

Figures 21 and 22 in the Appendix, pages 85-86, show X-ray scattering exposures of bovine serum albumin of concentrations of 15%, 5%, 1% and a background exposure with the sample chamber filled with water. These exposures were examined by a microdensitometer to obtain curves of optical density. These curves were calibrated against known optical densities and also against a curve of optical density versus exposure, obtained by taking known exposures of the central beam. A Guinier plot of the logarithm of the intensity versus h^2 was made from these data, and it gave the desired straight lines, proving that photographic detection is practical for this type of continuously distributed scattering pattern. In this case monochromatization is a strict necessity. There are serious disadvantages to photography for these continuous

curves, however, which make it necessary to adapt the apparatus for counter detection. In the first place the microdensitometer available could only be relied on to three percent accuracy, and the conversion from optical density to intensity required calibration curves. In addition to this the optical density of the film depends on the processing and developing of the film. This can only be controlled by calibrating each piece of film used with a standard X-ray intensity. The response of the film is different for different intensity ranges. For the one percent exposure of albumin the optical density was proportional to the intensity; for the other albumin exposures the density is proportional to the logarithm of the intensity. If the intensity is too large the film becomes uniformly black, and information is washed out. It is not necessarily known in advance how intense the scattering pattern will be, and this makes it difficult to determine the exposure time. More than one exposure may be necessary to explore the full intensity range of one pattern, which wastes valuable time when samples are perishable. Nearly all of the above factors combine to make background subtraction very difficult when the background intensity is at all comparable with the scattering intensity, as is the case for low concentrations and for the scattering region near the center of the patterns. Since low concentrations and low angles are both important in this work, some other method of detection is advisable. Similar difficulties arise in trying to measure accurately the intensity of the unscattered central beam. To the above difficulties may be added the fact that for the radial scanning of a circu-

larly symmetric pattern the counter method will usually be quicker than photography.

C. ADAPTATION OF THE INSTRUMENT FOR COUNTER DETECTION

1. Counter Installation for First Ribosome Series

A Geiger counter detector was installed in the instrument so that scattering patterns of large organic molecules in solution could be obtained more accurately. The first installation, used in the earlier ribosome runs to be described, is illustrated in fig. 6. The halogen-quenched, one-inch end mica window, argon-filled Geiger counter is housed in the cylinder C which contains lead around the counter so that background from cosmic rays and other sources may be minimized. This cylinder is suspended so that it will slide on the two stainless steel rods at A when moved by the micrometer screw at B. A slit is placed over the end of the Geiger tube, which is inside the instrument at the proper height to scan the pattern. The inside of the instrument was sealed from the outside at this end by a rubber diaphragm sealed to the underside of the plate and to the side of the Geiger tube cylinder.

This counter installation worked well with the narrow diffraction patterns obtained from ribosomes. For larger scattering angles, however, this arrangement is not satisfactory. Since the counter motion is wholly a translation, the scattered beam strikes the slit and counter at different angles than does the main beam. This will change the effective slit width for larger angles. For this reason a more satisfactory arrangement was constructed.

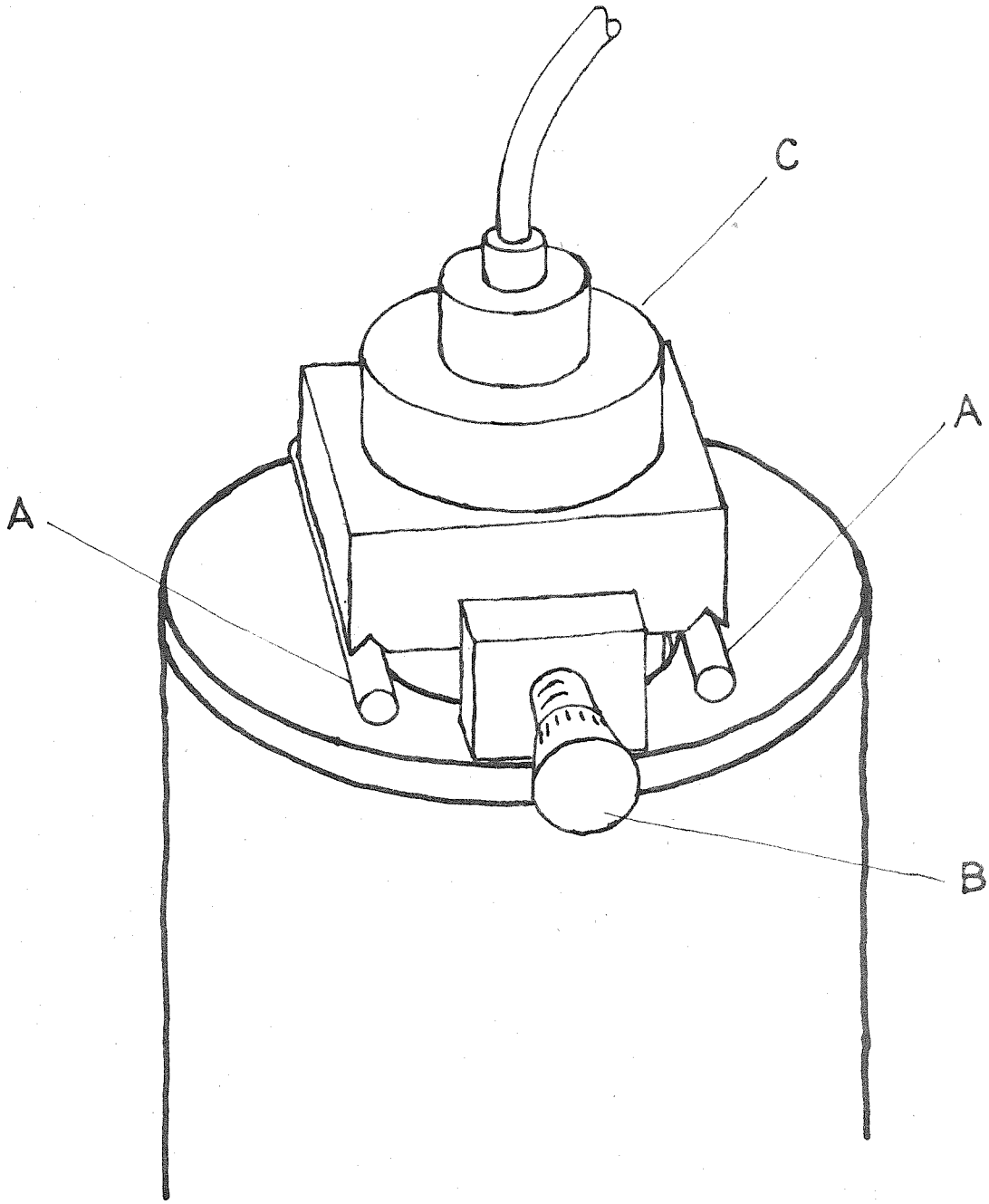

Fig. 6. Geiger counter installation for first series of ribosome runs. The end-window Geiger tube is within the lead-shielded cylinder C. This cylinder is fixed to the block which is pushed along the rods A by the micrometer screw B.

2. Counter Installation for Second Ribosome Series

Fig. 18 in the Appendix, page 82 , shows the adaptation of the instrument for counter detection finally adopted. The sample holder, slits, and detector are in air, while the beam path through the tube A is in helium. 0.0025 in. thick Mylar windows separate the helium path from the air and allow X rays to pass through with virtually no absorption. The diffusion of helium through these windows causes no trouble since there is a slow current of helium passing through the instrument at all times. To check the loss of helium and the diffusion of air into the instrument, the helium was turned off overnight. The intensity of the beam was essentially the same the next day, showing that a negligible amount of diffusion had occurred.

Samples and filters may be changed without disturbing the instrument in any other way. After the initial flushing out of the air with helium, very little helium is needed to keep the inside free from air. The instrument need only be opened up to adjust the crystal or the collimator, which ordinarily is not necessary. Since the sample is in air, there is no problem of helium diffusing into the sample, and organic films with little absorption for X rays may be used for the containing films in the sample frame.

The Geiger counter, shielded as before, and the tube A are attached to the two aluminum channel booms at B and move with them about the axis bb' through the sample position. The pivots of this rotation are fastened to the plate C which can be rotated so that the detecting system may be moved through any arc through the center of the pattern. A micro-

meter fastened to the steel post at D pushes against a ball bearing fastened to one of the booms to adjust the angle at which the scattering intensity is measured. A weight on a chord fastened to the boom and looped over a pulley on the post keeps the ball in contact with the micrometer. The space between the top of the sample holder and the bottom of tube A is sealed from the atmosphere with polyethylene film so that when the sample is cooled there will be no condensation of moisture in that region. The slit system fixed at the top of tube A achieves a square or rectangular aperture with which to explore the pattern by using two narrow slits at right angles to each other, placed one above the other. The entire slit assembly may be removed from the instrument exposing a Mylar window through which photographs may be taken if desired. The top of the slit assembly has three upright pins placed in it so that filters may be positioned in the beam.

3. Filters

Since the counter has a dead time of 480 microseconds, it is necessary to use filters to reduce the intensity of the more intense parts of the patterns on occasion, and of course the central beam. The crystal reflects integral multiples of the frequency that it is set for, according to the Bragg reflection condition, and these higher frequencies can be present in the continuous radiation incident on the crystal if the tube voltage is sufficiently high. Their intensities are of course much lower than that of the copper Kα line radiation, but these frequencies are in general more penetrating than the Kα line, and therefore may be important after the beam has been attenuated to a large degree with filters. For

this reason nickel filters are used, for which the absorption of the Kα line is less than that of its first harmonic, since the K absorption edge of nickel lies between them. The nickel filters used here gave results reproducible within a few per cent.

D. POSSIBILITIES OF INCREASED INTENSITY

Etching has been reported to reduce the intensity of reflection from quartz crystals by as much as fifty per cent. (16) This suggests that the intensity might be increased if the crystal were not etched. It was felt necessary to etch the crystal now in the instrument because of past experience with breakage and because this crystal had a long scratch in it. For an important enough application it might be worth the risk to etch the second crystal only on the edges and the side next to the metal block, leaving the reflecting surface unetched. This surface is not subjected to tension in the bending process, but only to compression, and chances appear good that it would survive.

This crystal was cut to use the 023 planes of quartz because they are close to the standard BT cut of the quartz crystal. The $02\bar{3}$ planes have the same Bragg angle as the 023 planes, and thus a crystal using them could be installed in the present instrument without requiring redesign or any alterations. The $02\bar{3}$ planes have been reported to have a reflection intensity 89/33 times as great as the 023 planes. (16) The use of these planes would give a sizable increase in the intensity of the instrument.

III. FIRST SERIES OF RIBOSOME RUNS

The rest of this work will be concerned with describing and interpreting scattering data taken on rabbit reticulocyte ribosomes. Ribosomes have become of increasing interest to biologists as evidence has become increasingly conclusive that these particles are the site of protein synthesis in living cells. These particles are about the same in size as the spherical virus particles, and are found in the plasma of the cell. They are composed of ribonucleic acid (RNA) and protein in approximately equal amounts.

Ribosomes were obtained from Dr. Howard Dintzis prepared using the method described by Dintzis, Borsook, and Vinograd(18). The ribosomes were dissolved in a substrate of water containing 0.14 M KCl, 0.001 M $MgCl_2$ and 0.01 M trischloride buffer. It was felt that in order to obtain enough intensity to take data on low concentrations it would be necessary to scan the patterns with an "infinite" slit. Accordingly, a slit 0.4 in. in height and 0.013 in. in width was placed in front of the Geiger counter. The counter was an end window, halogen-quenched argon-filled counter, with mica window diameter one inch.

A. DATA TAKING PROCEDURE

1. Background

There are three possible sources of background, excluding the cosmic ray and other general background sources. The first of these is the scattering from the substrate in which the sample is dissolved. This will vary with the amount of substrate present, and like the scattering from the sample itself does not vary much with the thickness of the

sample, providing the sample and substrate combined absorb nearly 1/e of the beam. This scattering may be appreciable when larger slits are used, but in the present case seems to be almost negligible. The second part of the background is the scattering from the film containing the sample. In the case of mica this proved too small to be reliably detected, but the Parafilm scattering is not negligible. The most important part of the background arises from radiation in the incident beam coming from the crystal and collimator, especially for such scattering experiments as with ribosomes where much of the pattern is close to the central beam. Both of the last two contributions to the background are proportional in magnitude to the intensity in the central beam after coming through the sample. Thus the proper way to match a background value for subtraction from a scattering curve is as follows: take the value for a run in which the sample holder is filled with substrate alone, and raise or lower it proportionally with the ratio of the intensity of the central beam of the sample run to the value for the background run. This procedure was followed for this series of runs. The substrate run was done after the last of the ribosome runs.

2. Taking and Processing of Data

The cooling system was used in this series of runs to hold the temperature of the sample within a degree or two of zero degrees centigrade.

The dead time of the counter used in this experiment was measured by a variation of the two-source method. The X-ray beam was split into two beams by means of a lead mask with two holes in it put across the beam. The counter at the focus measured the intensity through each

of the two holes separately and then both together. By this method any change in the apparent dead time due to the pulsed output of the X-ray tube need not be computed, since the dead time needed is the dead time measured. This dead time was 480 microseconds, to limits of accuracy of the measurement, and the correction to the counting rate was obtained using curves published by Taylor (19).

First the scattering data were corrected for the dead time of the counter. Then the cosmic ray or "external" background, as measured by the counter with the beam turned off or blocked off with lead, was subtracted from the data. This amounted to about 22 counts per minute. Next any adjustment needed because of absorbers in the beam was made. Following this the substrate background was adjusted as described above and subtracted from the values of the scattering data, which were then plotted as in fig. 7.

The sample holder was weighed on an analytical balance before and after filling in order to determine the mass in each sample. The intensity over the central beam was measured, with the necessary absorbers in the beam, with the same slit used to scan the scattering pattern. These quantities are tabulated in table II which also gives the concentrations and other data on the samples. A slight drift in the position of the central beam was noted from run to run, and corrected for where necessary. The sample-to-film distance was 47.95 cm.

B. INTERPRETATION OF DATA

1. Search for Secondary Maxima

Figure 7, which shows the scattering curves obtained, also

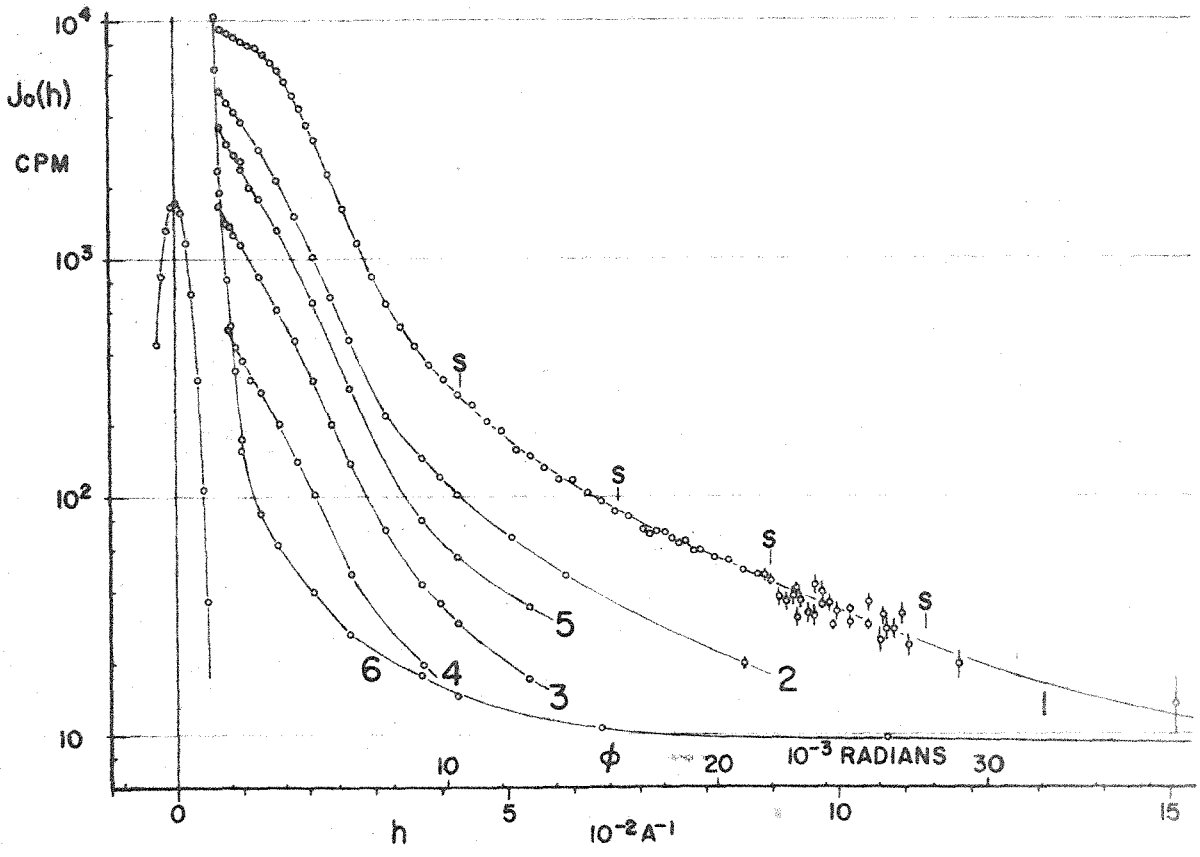

Fig. 7. Scattering curves for first series of ribosome runs. The points marked S correspond to maxima in the ideal scattering curve for a sphere of uniform density of the same radius of gyration as the ribosome particle. The limits shown are plus or minus the standard deviation determined from the counting rate. These are shown where greater than the dimensions of the circles marking the experimental points. The standard deviation for the points in finding the radius of gyration was one per cent except in the region of very high background.

shows the location at which one would expect to find the secondary maxima for a sphere of the radius of gyration determined in the next section. The maxima expected will be at slightly different positions from those indicated, since the use of the infinite slit geometry displaces them. It was originally hoped that these maxima would aid in determining the size of the particle, as was done with virus particles by Beeman and his coworkers (5, 6). However, it is clear that these maxima and minima do not occur in these data. It does not seem to be possible to account for their non-appearance by nonuniformity of the sample or smearing of the slits. It must be remembered that the presence of these maxima and minima are predicted (and observed) for a sphere with uniform density and therefore a sharp change of density on the boundary. It is likely that there is no sharp change of density on the boundary of this particle, but a more gentle change from the density of the particle to the density of water. Virus particles are in an inactive state, and thus are surrounded by a hard surface, which gives the secondary maxima; while the microsome particle is in something similar to its active protein-producing state.

2. Determination of the Radius of Gyration

The scattering data were used to determine the radius of gyration of the particle. Figure 8 shows the plot of the logarithm of intensity versus h^2. It can be seen from the figure that the Gaussian approximation is accurate over an appreciable region of the scattering curve. The curves depart from straight lines at small angles where the background is high, and where also interparticle interferences should be important, and also at larger angles. The slopes of the curves were measured and from them values of the radius of gyration calculated. These

TABLE II

Run Number	Concentration Ribosome g/ml	Weight, Grams	Center of Central Beam in Air x 10^{-6} in Counts Per Minute	Apparent R_o	dR_o/R_o from Errors in h (%)	% dR_o/R_o from Statistics	Estimated Plotting Error	dR_o/R_o from 10% Error in Background	Estimated Total Error
1	.113	.8008	5.43	102.3	.2	1.2	.70	.07	2%
2	.038	1.1191	5.46	106.6	.2	.9	.35	.04	1.5%
3	.0113	.7118	5.43	105.0	.2	1.1	.35	.05	1.5%
4	.0038	.7272	5.19	109.3	.2	2.1	.60	.25	3%
5	.023	.6654	6.34	104.3	.2	.9	.35	.06	1.5%
6	0	.6932	5.94						

values are tabulated in table II. In order to eliminate as much as possible the effects of interparticle interferences, these values must be extrapolated to zero concentration. This is done by means of the curve in fig. 9. The extrapolated result is the value of 106.5 A for the radius of gyration.

Correction for Slit Width. As mentioned in Part I, there is no correction for slit height necessary in determining the radius of gyration. However, there is a correction necessary for slit width. Equation 9 may be solved, as shown by Guinier (2), by taking the Fourier transform of both sides and solving for the Fourier transform of J(h). In the present case, since the correction to a Gaussian is required, the obvious method is to take a Gaussian for the central beam profile, adjusted to have the same half-width and total intensity. If we have:

$$j(h) = \frac{d}{2\pi} \exp\left(-\tfrac{1}{2}(hd)^2\right) \tag{19}$$

$$J_o(h) = A \exp\left(-\tfrac{1}{2}(ha)^2\right) \tag{20}$$

Then:

$$J(h) = P \exp\left(-\tfrac{1}{2}(hp)^2\right) \tag{21}$$

Where:

$$p = \frac{ad}{(d^2 - a^2)^{\frac{1}{2}}} \tag{22}$$

$$p = \frac{pA}{d} \tag{23}$$

and the corrected radius of gyration R_o

$$R_o = R_o' \left(1 - a^2/d^2\right)^{-\frac{1}{2}} \tag{24}$$

Here R_o' is the radius of gyration obtained if no slit width correction is

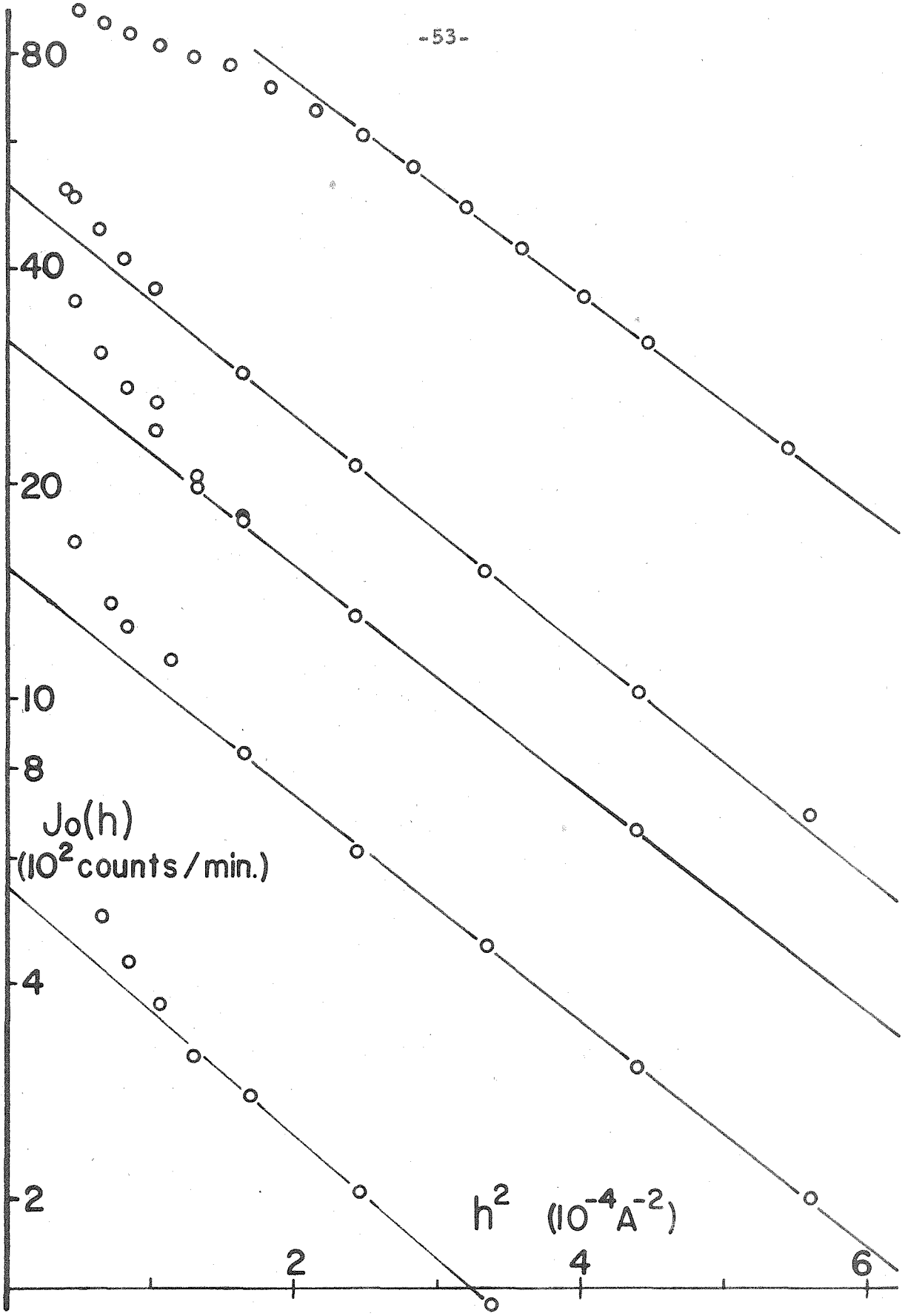

Fig. 8. Plot of logarithm of intensity vs. h^2 for 1st ribosome series.

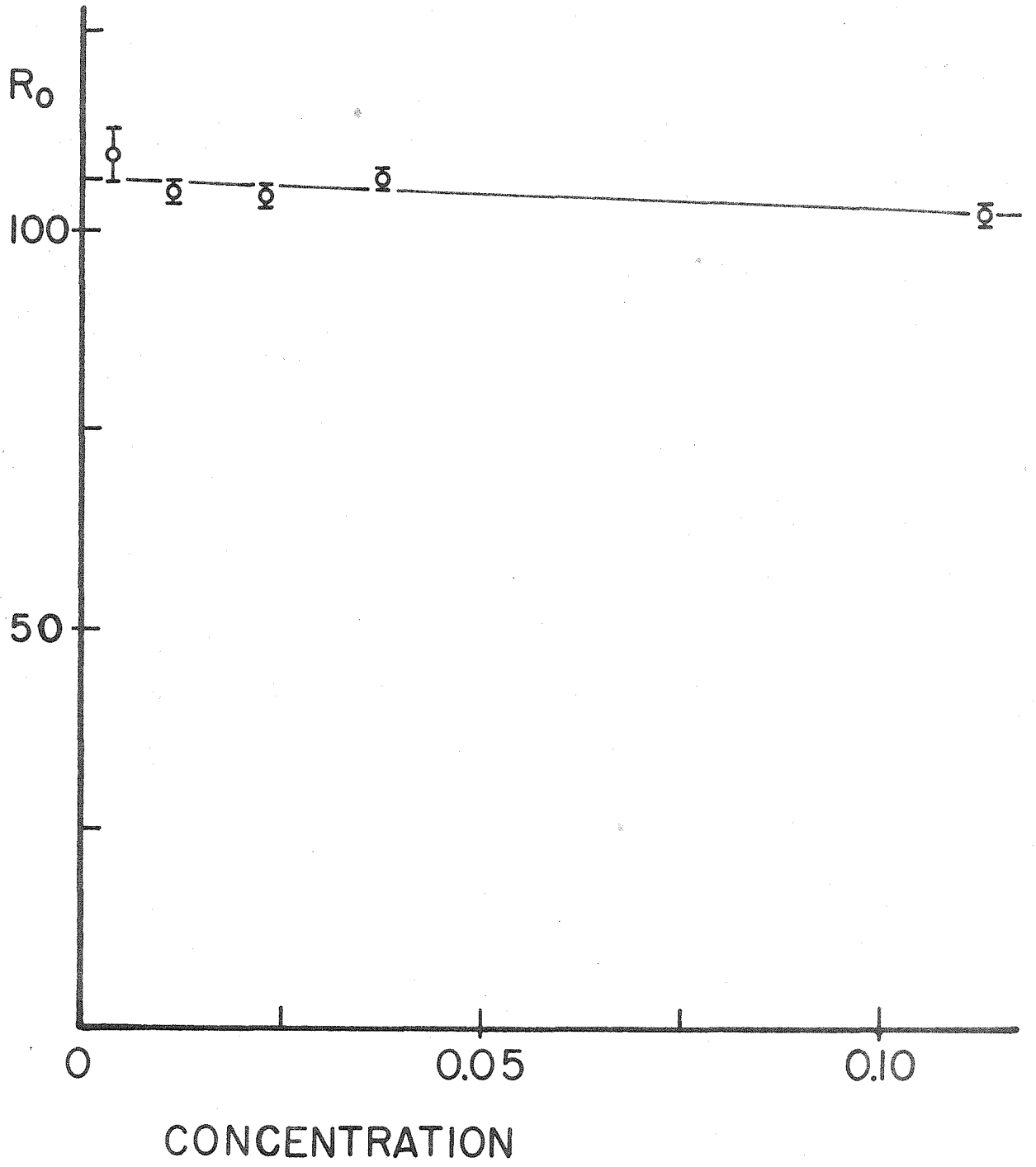

Fig. 9. Plot of R_o, the apparent radius of gyration in angstroms, versus the concentration of the ribosome solution in g/ml for the first series of ribosome runs. R_o is obtained from the curves of fig. 8 at each concentration. Estimated errors are indicated.

applied. The corrected radius of gyration is 107.8 A.

Estimation of Error Due to the Presence of Aggregates. Rabbit reticulocyte ribosomes prepared in the method used here contain particles larger and smaller than average. The approximate amounts are found by use of the ultracentrifuge and are not precise, but amount to nine per cent heavier particles, presumably aggregates, and another nine per cent lighter particles (18). The presence of smaller particles has much less effect on the radius of gyration measured in this way than the heavier particles, since the method favors larger particles in the average radius calculated. Therefore, it was considered necessary to check the influence of larger particles on the present results.

For very large particles, the scattering should be at extremely small angles and hence would not affect our results. The difficulty should arise from the presence of small aggregates. Considering the aggregated portion of the sample to consist entirely of dimer, we can estimate the amount of scattering this would cause. The radius of gyration of the dimer can be calculated, and then the scattering caused by a particle with this radius of gyration can be compared with that caused by the single particles. If this is done, we find that the radius of gyration we have measured should be about 2.5 per cent too high in the region of our best data on the logarithm of intensity versus h^2 plot, leaving us with a best value of about 105 A.

Effect of Statistical Counting Errors. An estimate of the effect of statistical counting errors on the value obtained for the radius of gyration is obtained by considering the straight line on the logarithm intensity

versus h^2 plot to be determined by two intensity values at points where the background is small. This has been calculated, and the results are tabulated in table II. The values given are clearly upper limits for the error, since many points were taken to determine the straight line, and therefore the actual errors should be significantly lower than indicated.

Error in Background. The value of the radius of gyration will be affected by an error in the intensity of the background subtracted from the scattering curves. The effect of an error of ten per cent in the background intensity was calculated. The background was taken at two points in the linear region of the logarithm intensity versus h^2 curve and the effect of a change of ten per cent of these values was considered. The results are tabulated in table II and are surprisingly small. Apparently the background curve under the scattering curve varies with h in such a way that the error considered here is small.

The possible sources of error, tabulated in table II, all give errors less than the uncertainty in the radius of gyration caused by the presence of aggregates. The error caused by uncertainty in the measurement of h is negligible. Except for the aggregation problem, the radius of gyration given should be accurate to about two per cent.

3. Estimation of the Molecular Weight

For each run the intensity distribution in the central unscattered beam was measured by scanning it with the same slits used in measuring the intensity distribution of the scattering pattern, using, of course, nickel filters to attenuate the beam. The total power in the beam was measured by integration of this intensity distribution. This makes it

possible to estimate the molecular weight of the particle using equation 13. Other information is also necessary to make this calculation.

The intensity at zero angle for an infinite slit may be obtained by extrapolation by using the Gaussian obtained as a result of the slit width correction. Because the value of the radius of gyration determined from the third ribosome run corresponds with the radius of gyration obtained as the best value computed, it was decided to use the curve of run three to obtain the extrapolated intensity at zero angle. This then was subjected to the slit height correction of equation 10, which may be readily done for a Gaussian, obtaining the intensity scattered at zero angle as seen by an ideal point aperture. This gives $I(0)$.

The total number of electrons in the mass of the sample was obtained from the mass given in table II and from the chemical composition of the ribosome (20). This may be converted to the total number of electrons in excess of the electron density of water by using the partial specific volume of the ribosome particles of 0.63 milliliters per gram (18).

An intensity for the incident beam at the scatterer was obtained by dividing the power in the beam as measured after passing through the sample by a cross-sectional area of the sample, i.e., of the window in the sample frame. Measuring the power in the beam after it goes through the sample automatically corrects for the losses by absorption in the sample, since this gives precisely the correct beam to cause the observed scattering from the measured mass of the sample if there were no absorption. This assertion assumes the scattering angles and scattering cross-sections small as is true in the present case. A calculation will

confirm this, but it can be seen intuitively by noticing that any photon emerging from the sample in either the scattered or unscattered beam has had the same probability of absorption. This means that the intensity distribution with absorption is merely a reduction by a constant factor of that without absorption. The cross-sectional area used in calculating the incident intensity is incorrect, since the beam doesn't impinge on the entire window of the sample frame, as is obvious from an exposure of the beam with the film in the sample position as shown in fig. 19 in the Appendix, page 83. However, this same area is used implicitly in using the entire mass of the sample as the scattering mass, since the mass irradiated is proportional to the irradiated area of the sample window. The area thus cancels out of the calculation. This may also be seen intuitively from the fact that the scattering will not depend on whether or not the beam is concentrated or spread over the sample.

The measurements and extrapolations necessary for this measurement are not all accurate, and the result should not be reliable to better than 20 per cent. The main problem is in extrapolating the steep Gaussian to zero angle, with most of the center cut off from experimental access. Inaccuracies in the measurement of the central beam also contribute. The value obtained excludes the nine per cent of aggregated particles, since the Gaussian used does not include the effects of such aggregation. The presence of about nine per cent of the mass of the sample in the form of smaller particles does affect the estimate of the mass of the particles. A correction for this effect was made assuming that the nine per cent of smaller particles was comprised of the larger subunits to be discussed in Part III. These subunits have a mass of about one-third of

the mass of the ribosome particle. The effect of this correction was to raise the measured value by 3.4 per cent.

The value obtained for the mass of the ribosome particle after the corrections described above was 6.7×10^{-18} grams. This corresponds to a molecular weight of 4.1×10^{6}. This value of the molecular weight compares surprisingly well with values calculated from the results of other experimental methods. Results of sedimentation, viscosity, and partial specific volume measurements indicate a molecular weight of 4.1×10^{6} and results of light scattering experiments show a molecular weight of 4.0×10^{6} in solutions(18). Electron microscope results, to be discussed later, indicated a molecular weight for the dry particles of 3.7×10^{6}. In view of the extensive hydration of the ribosome particle to be discussed later, this last result might seem at first to contradict the others which give essentially the same result for particles in solution. However, the X-ray results were calculated with the partial specific volume obtained by the dissolving of a known weight of the particles and observing the increased volume of solution; not the actual specific volume of the particles in solution. Thus the molecular weight measured here is also the dry molecular weight, which is well confirmed by the results of the other sources.

The use of this method of measuring the weights and molecular weights of particles does not seem to have been used as often as it warrants, probably because of the inconvenience and difficulty of measuring the intensity of the central beam and also the difficulty of extrapolating curves to zero angle accurately. Nevertheless, the X-ray method appears to be reliable, has the advantage of being a direct measure of the

particle, and gives the molecular weight in conjunction with other accurately measureable quantities. The present results, although only approximate, give confidence in the feasibility of the method.

IV. SECOND SERIES OF RIBOSOME RUNS

It has been observed by T'so and Vinograd that there is a large increase in viscosity and sedimentation constants of ribosomes when the ionic strength of the solution is decreased almost to zero by dialysis(21). This change could be caused by an increase in the volume of the particles, or by some other effect that would reduce the available volume of solution open to the particles by a factor of two or three caused by increased hydration or increased mass of the particles. Since at low or zero ionic strength the particles are no longer shielded by the ions in the solution, the coulomb interaction between the charges on the ribosome particles causes a repulsion between the particles which can effectively increase the volume of solution "occupied" by one particle, even if the particle itself does not change in volume. Since X-ray diffraction, except for interparticle interaction effects which can be extrapolated out in favorable cases, "sees" directly the excess electron density of the particle, the scattering method should be able to answer this question. Accordingly, four more runs were taken on rabbit reticulocyte ribosomes furnished by Dr. Paul T'so. Added complications arose from the aggregation and degradation of the particles, which are dependent on the magnesium ion concentration. In salt solutions,with magnesium ion present, of these ribosomes there is generally about 10 to 15 per cent aggregation, and a few per cent degradation products. In the magnesium-free low-ionic-strength solutions the degradation products are about the same, but there is essentially no aggregation. In addition to this, about 20 to 40 per cent of the ribosomes break up into subunits, each breaking up into two subunits, one of which comprises two-thirds of the mass of the particle(21).

Low concentrations were used in this series of runs, less than 1.5 per cent, in order to avoid any possible changes in the particles that might be caused by centrifuging down to a pellet and redissolving. The particles were centrifuged just before the first run in an effort to remove as many aggregates as could be conveniently eliminated. This means that the first run in this series probably contained the purest sample of ribosomes investigated here.

Four samples of ribosomes were investigated. The first two, runs A1 and A2, were in a salt solution containing 0.05 M KCl, 0.0015 M $MgCl_2$, and 0.001 M trischloride buffer. These were at concentrations of 1.3 and 1.0 per cent respectively. The second two samples, runs B1 and B2, were in a solution from which salt had been removed by dialysis but which was still 0.001 M in trischloride buffer. They were at concentrations of 1.1 and 0.55 per cent respectively. Data were taken at room temperature and the samples were kept in the refrigerator between runs.

The scattering curves were investigated by scanning with a slit 0.013 in. in width and 1/32 in. in height. Background runs were taken before and after the series of four runs. A volume of 0.61 milliliters of sample solution or substrate, as measured by syringe, was used as sample in each run. The weight of each was also measured. A distance of 47.9 cm was used between the sample and the exploring slits. Table III lists some of the above data.

Ribosomes from sample A1 were investigated in the ultracentrifuge after the X-ray data were taken and showed from 10 to 15 per cent aggregation and about 5 per cent degradation. (These figures are of course approximate.) There was no evidence of the presence of subunits. Sample

B2 was similarly investigated and showed no aggregation, and about 5 per cent degradation products. It also showed about 35 to 40 per cent dissociation into subunits. These values may be larger than those holding during the time the first X-ray results were obtained, as the centrifuge data were taken several days afterwards. Nevertheless, they show about what is to be expected from such solutions.

The instrumentation and background subtraction were essentially the same as on the first series. A new counter was used, which proved to have the same dead time as the old one, but had an external background of only about 17 counts per minute. The background was somewhat higher in this series since in the first series the collimator had been canted reducing the intensity but also cutting the background on the side of the beam on which data were taken*. This was not done in the second series. Because of low concentrations and also the use of slits of smaller cross-sectional area, as well as the higher background, the intensity above background as well as the total intensity of this series was lower than the first. Therefore, the accuracy of this series was not as good as that of the first.

The curves of the logarithm of the intensity versus h^2 are plotted in figs. 10, 11, and 12. The radii of gyration obtained from the slopes of

---

* The collimator may be turned slightly in the beam so that the vanes converge from the crystal to a point slightly off the X-ray focus, P_2, instead of converging directly to the focus itself. This will result in less collimation and thus higher background from the halo on the side of P_2 toward which the collimator is focused. On the other side, however, the background is lessened. There is, of course, some lessening of the intensity of the unscattered beam, but this loss is more than compensated for by the decrease of background in the very low angle region.

Run	Back. 1	A1	A2	B1	B2	Back. 2
KCl Molality	0.05	0.05	0.05	0.0	0.0	.005
$MgCl_2$ Molality	0.0015	0.0015	0.0015	0.0	0.0	.0015
Ribosome Concentration %	0.0	1.3	1.0	1.1	.55	0.0
Aggregation Products	-	10-15%	15%	0	0	-
Dissociation into Subunits	-	0	0	35%	35-40%	-
Degradation Products	-	25%	25%	25%	25%	-
Trischloride Molality	.001	.001	.001	.001	.001	.001
Volume of Sample Solution, ml	.61	.61	.61	.61	.61	.61
Mass of Sample Solution, grams	.6032	.6073	.6048	.6027	.6046	.6007
Power in Central Beam x 10^{-8} in counts per minute		3.47	3.5	3.7	3.55	
Uncorrected Radius of Gyration in A		100.2	103.4	98.6	101.2	
Molecular Weight x 10^{-6}		1.69	1.86	1.75	2.03	

TABLE III.

Data on Second Ribosome Series

these curves and also the molecular weights obtained from the intercepts are listed in table III.

The radii of gyration obtained agree very well with each other and also with the results of the first series of ribosome runs. It is somewhat surprising how far the Gaussian region of the curve extends, particularly for run A1. Since runs A1 and A2 were taken on the samples which showed no evidence of breakdown into subunits, it is expected that the curves are correct except in the very low-angle region where the aggregation effects are noticeable. This expectation is well justified by the appearance of the curves. The radii of gyration obtained from curves A1 and A2 should not be as much affected by the aggregation as those from the first series, since it is possible to use points on the Gaussian at high enough angles so that the scattering from aggregation products is negligible. Thus, with the slight increase due to slit correction, the values obtained are in excellent agreement with the previous results. The slightly lower values obtained from runs B1 and B2 are to be expected from the effects of the presence of considerable quantities of subunits, which slightly lower the measured value of the radius of gyration. It is interesting that the curves have a slightly higher slope in the very low angle region, where the scattering from the subunits would have much less effect. Thus, the data are consistent with the contention that there is no change in the radius of gyration as a result of the change of ionic strength.

The absolute values of the molecular weights obtained from this series of ribosome runs present a problem, although the relative values confirm the conclusions of the preceding paragraph. The values are all

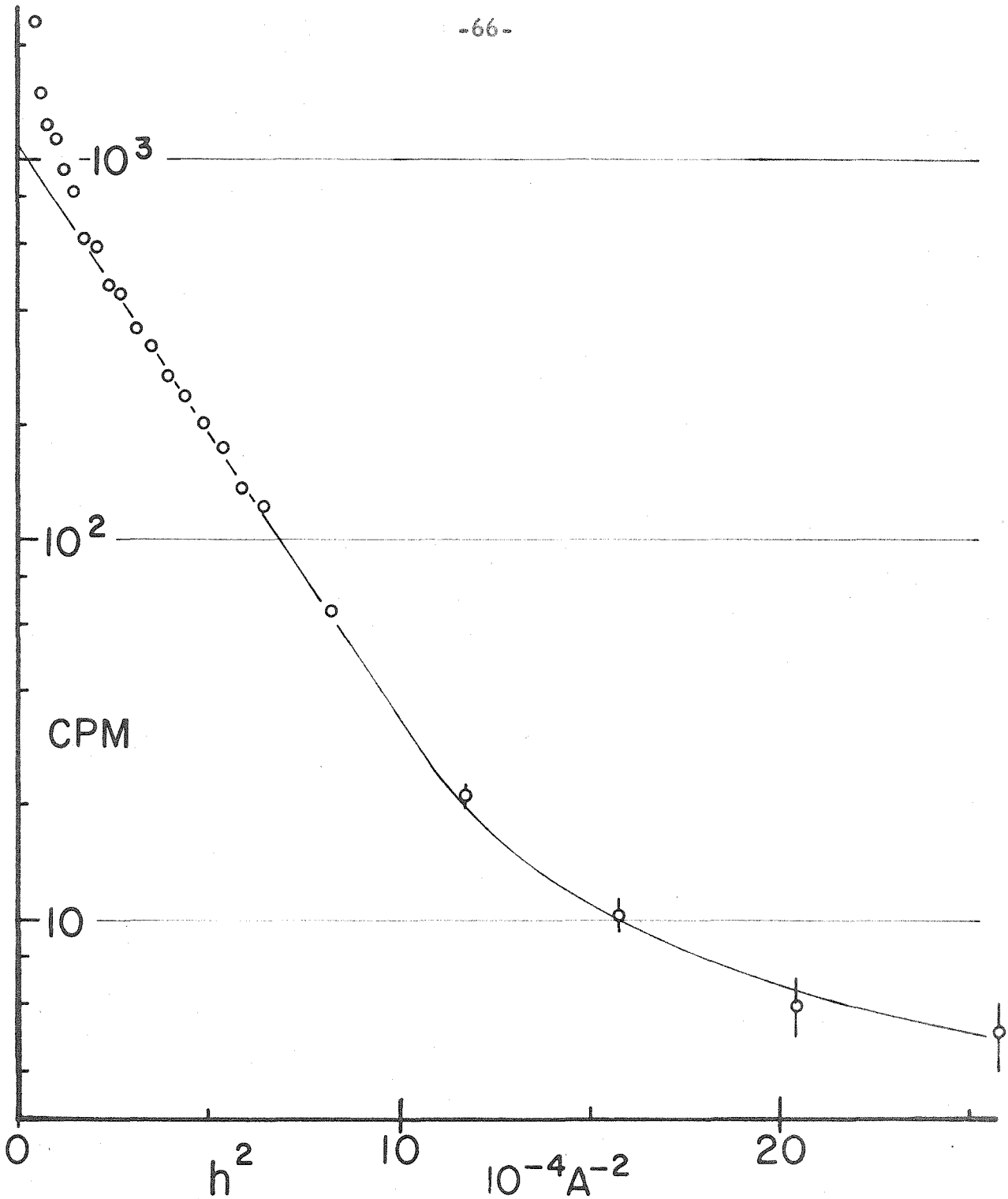

Fig. 10. Plot of the logarithm of the intensity versus h^2 for the first run, A1, of the second series of ribosome runs.

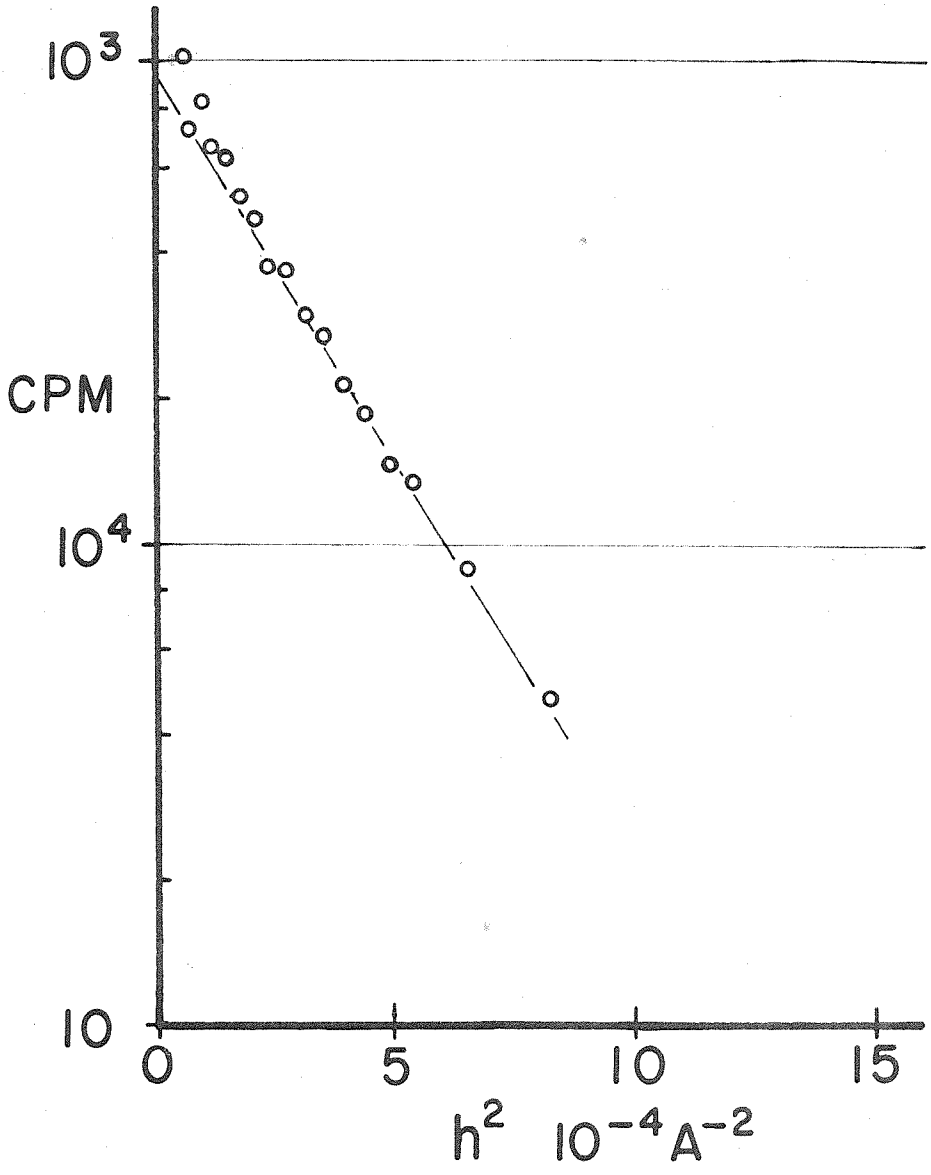

Fig. 11. Plot of the logarithm of the intensity versus h^2 for the second run, A2, of the second series of ribosome runs.

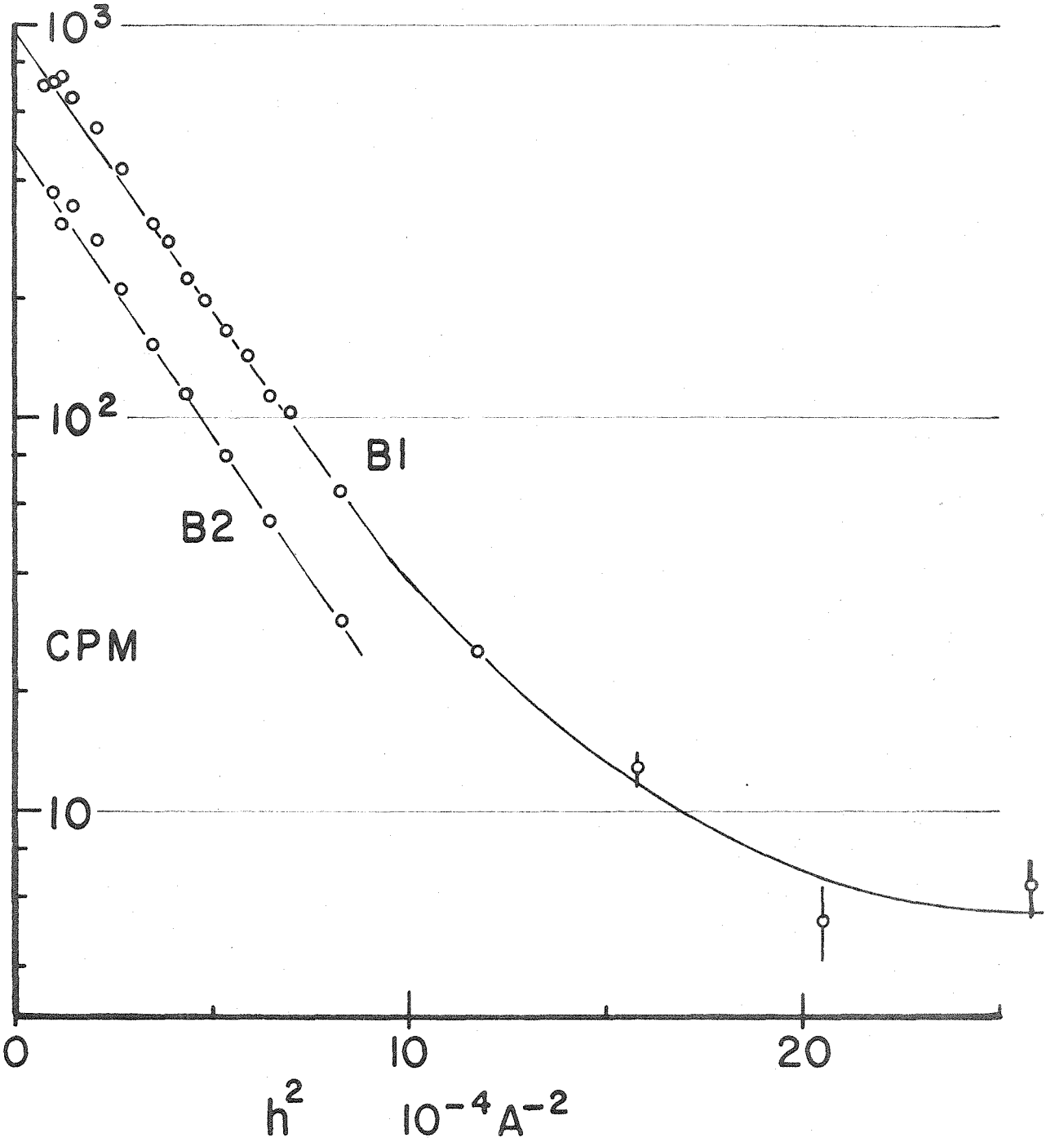

Fig. 12. Plot of the logarithm of the intensity versus h^2 for the third and fourth runs, B1 and B2, of the second series of ribosome runs.

about a factor of two less than those obtained in the first series, and this result is so far without satisfactory explanation*. However, the values obtained for these four runs agree well among themselves. The values listed in table III have been approximately corrected for the presence of aggregates and subunits. They are all equal within the limits of experimental accuracy, and thus this result is also consistent with the contention that there is no change of size with ionic strength.

If there is a change of size with ionic strength, it must be of such a nature that the radius of gyration changes by about five per cent or less. This would correspond to a change of volume of about fifteen per cent or less, providing that there were no accompanying change of shape. If the expected expansion is to consist of an increase in hydration of the particle, then no change in the dry molecular weight measured by this method would be observed. Only if the particle should change its volume without change in hydration would there be an observed change in the intercept

---

* This result has so far defied all attempts to explain it on the basis of faulty calculations or systematic instrumental error, which would at first seem the most likely explanation. It would seem very unlikely that the dry molecular weight changes by a factor of two between the ionic strength used in the first series of runs and the lower ionic strengths used in this second series. It should be noted that the partial specific volume used in calculating the molecular weights was measured in the higher ionic strength substrate of the first series of runs, and therefore may not be correct for the second series. An increase of twenty per cent in the partial specific volume would account for the decrease in the molecular weight observed, but since the particle is highly hydrated, this would change the radius of gyration by less than two per cent, which would not be noticeable. Whether this is the correct explanation for this anomalous effect must be decided by future experiments which will be carried out as soon as the instrument is again available. Since the earlier result is more accurate, agrees with the results of other methods, and since there is no question but that it used the correct partial specific volume, it will be used in the following discussion.

of the curve. The present data imply that any such change must be less than about twenty to thirty per cent. Thus the results of the X-ray scattering experiments indicate that the results obtained in the viscosity and sedimentation experiments must be due mainly to coulomb interaction of the particles at the lower ionic strength.

V. DISCUSSION OF THE RIBOSOME RESULTS*

Some of the results of the work done here on the rabbit reticulocyte ribosome aid in understanding the nature of this particle. The best value of the radius of gyration obtained in this work is 105 angstroms. Also, the molecular weight has been approximately measured at 4.1×10^6, in good agreement with results from other methods.

Electron microscope pictures of these ribosomes have been taken by Professor Cecil Hall of the Massachusetts Institute of Technology. These pictures showed the ribosomes to be almost spherical with a diameter of 200 angstroms and a height of 185 angstroms (22). These dimensions are for the dried particles, and correspond to a dry volume of 3.9×10^6 cubic angstroms and a molecular weight of 3.7×10^6.

Light-scattering data also show the particle to be almost spherical, with molecular weight of 4×10^6 and diameter of about 340 angstroms (18).

If we conclude from the light-scattering and electron microscope data that the particle is approximately spherical, then it becomes reasonable to consider the particle to have spherical symmetry as a first approximation to its density distribution. A model based on a sphere of uniform density is not appropriate because of the lack of subsidiary maxima on the scattering curve. Since the results of the second series show the scattering curve to be a Gaussian out to comparatively large angles, an approximation to the electron density distribution of the particle may

---

* Some of the following has been published in a preliminary note by the author in collaboration with Dr. Howard M. Dintzis (22).

be made by taking the Fourier transform of this Gaussian. Since the radius of gyration is known, and the Fourier transform of a Gaussian is a Gaussian, the electron density distribution of the particle may be approximated by a Gaussian of the radius of gyration of the particle. An appropriate cutoff must be selected since the density of the particle does not extend to infinity. Figure 13 shows a Gaussian with the same radius of gyration, 105 angstroms, as the ribosome particle. The radius, R_s, of a sphere of uniform density of that radius of gyration is also indicated. R represents the cutoff, approximately 170 angstroms, obtained by extending the tangent at the point of inflection to the horizontal axis.

Let us consider the ribosome in solution to be a uniformly hydrated sphere, such that all the volume within the particle that is not taken up by the ribosome protein or RNA is taken up by water of hydration. Using the radius of 170 angstroms obtained above, a volume of 20.5×10^6 cubic angstroms is obtained. If this dries down to the volume observed by the electron microscope, then there is obtained a value for the hydration of the wet particle of 2.7 grams water per gram ribosome.

This value is in good agreement with a value of 2.6 grams water per gram ribosome obtained from data on sedimentation, viscosity, and partial specific volume (18). This leads to the picture of the ribosome particle in solution as an almost spherical sponge-like structure, with most of its volume as water of hydration.

If the value for the mass of the particle obtained from the intercept at zero angle of the scattering curve in the first series of runs is com-

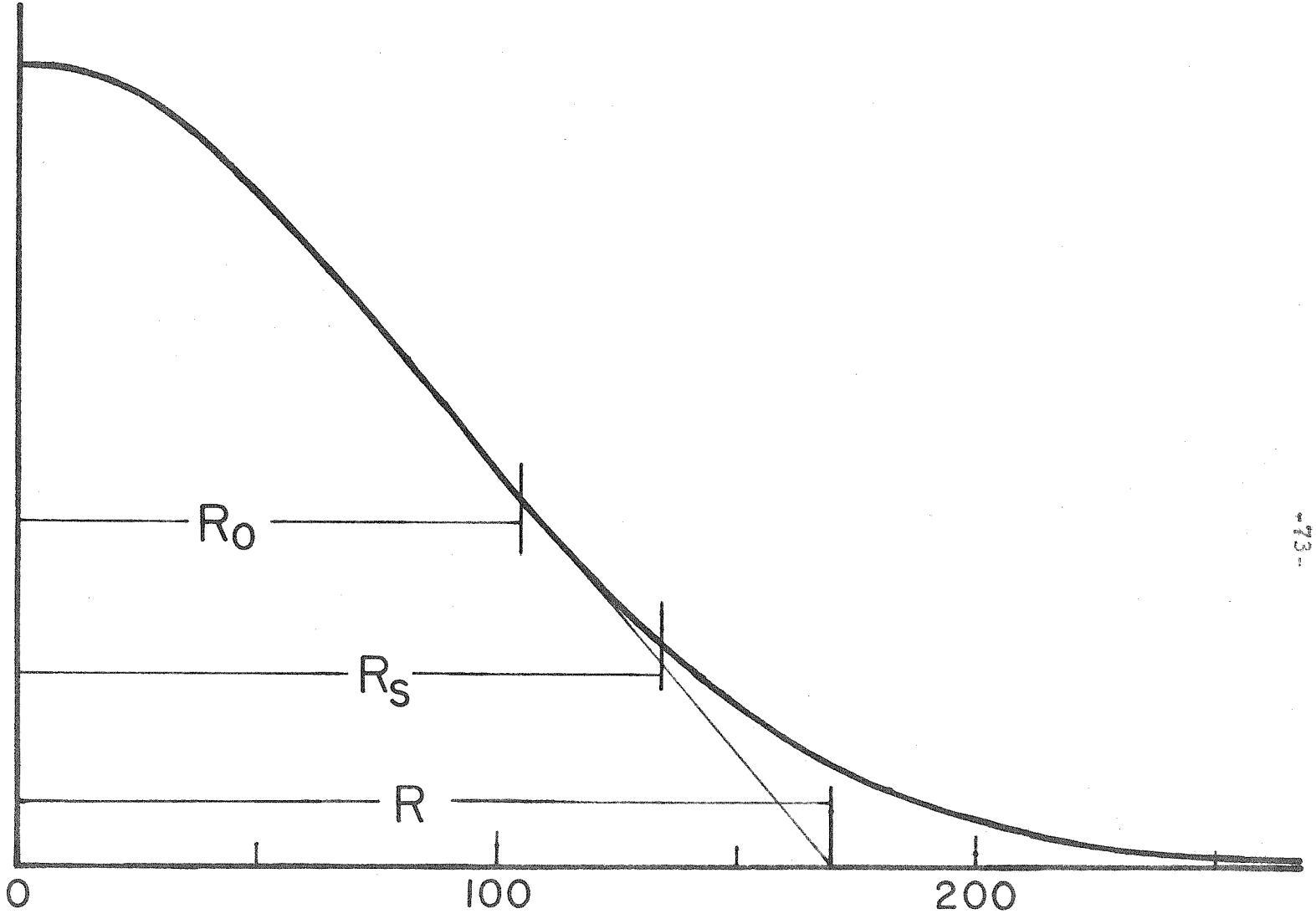

Fig. 13. Gaussian with same radius of gyration, R_o, as ribosome particle. R_s is the radius of a uniform sphere of the same radius of gyration. R is taken as the cutoff. Abscissas are in angstroms.

bined with the value of the partial specific volume, corrected for the hydration of the particle, a volume for the particle in solution of 22×10^6 cubic angstroms is obtained. This is consistent with the results calculated from the radius of gyration.

Ribosomes from different sources appear to be similar to each other (20)(23). Anderegg has reported on X-ray scattering studies of several other ribosomes, from A. Vinelander, yeast, and azotobacter(24). A radius of gyration of 114 angstroms was reported for yeast. No subsidiary maxima were observed for the ribosomes studied, which agrees with the results obtained here on rabbit reticulocyte ribosomes.

REFERENCES

1. A. Guinier, G. Fournet, C. B. Walker, and K. L. Yudowitch: Small-Angle Scattering of X-Rays, (1955), John Wiley and Sons, Inc., New York.

2. A. Guinier, et al: reference 1, page 113.

3. J. W. M. DuMond: Phys. Rev., (1947), 72, 83-84.

4. W. E. Danielson, L. Shenfil, and J. W. M. DuMond: J. Appl. Phys., (1952), 23, 860-865.

5. B. R. Leonard, J. W. Anderegg, S. Shulman, P. Kaesberg, and W. W. Beeman: Biochim. et Biophys. Acta, (1953), 12, 499-507.

6. P. Schmidt, P. Kaesberg, and W. W. Beeman: Biochim et Biophys. Acta, (1954), 14, 1-11.

7. A. Guinier, et al: reference 1, page 24.

8. A. Guinier, et al: reference 1, page 133.

9. J. Despujols: Compt. rend., (1952), 235, 716.

10. D. W. Berreman, J. W. M. DuMond, and P. Marmier: Rev. Sci. Instr., (1954), 25, 1219.

11. D. W. Berreman: Rev. Sci. Instr., (1955), 26, 1048-1052.

12. J. W. M. DuMond and H. A. Kirkpatrick: Rev. Sci. Instr., (1930), 1, 88-105.

13. H. H. Johann: Z. Physik, (1931), 69, 185-206.

14. D. W. Berreman: Doctorate thesis, California Institute of Technology, (1955).

15. J. W. Anderegg, W. W. Beeman, S. Schulman, and P. Kaesberg: J. Am. Chem. Soc., (1955), 77, 2927-2937.

16. C. Barclay and L. T. Sogn: Reference Data for Orienting Quartz Plates by X-Ray Diffraction, (1953), National Bureau of Standards, Circular 543.

17. J. W. M. DuMond, D. A. Lind, and E. R. Cohen: Rev. Sci. Instr., (1947), 18, 617-626.

18. H. M. Dintzis, H. Borsook, and J. Vinograd: Microsomal Particles and Protein Synthesis, (1958), Washington Academy of Sciences, Washington, D. C., page 95.

19. D. Taylor: The Measurement of Radio Isotopes, (1951), John Wiley and Sons, Inc., New York.

20. P. O. P. T'so, J. Bonner, and H. Dintzis: Arch. Biochem. Biophys., (1958), 76, 225-227.

21. P. O. P. T'so and J. Vinograd: to be published.

22. W. E. Dibble and H. M. Dintzis: Biochim. et Biophys. Acta, (1960), 37, 152-153.

23. P. O. P. T'so: Structure of Microsomal Nucleoprotein Particles from Pea Seedlings, (1958), Washington Academy of Sciences, Washington, D. C., pages 156-168.

24. J. W. Anderegg: Program and Abstracts, Biophysical Society 1959 Meeting, Pittsburgh, Pennsylvania.

APPENDIX

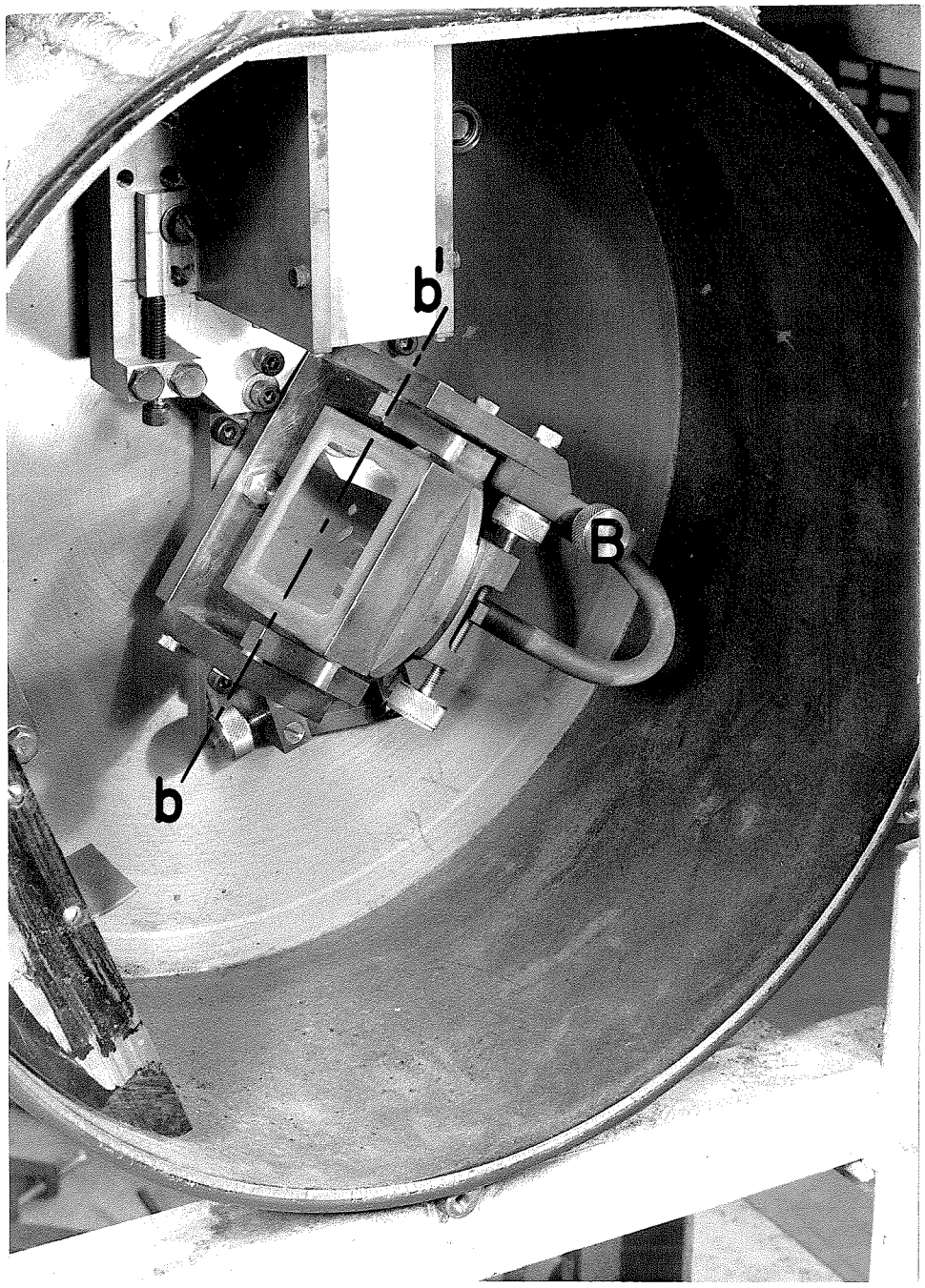

Fig. 14. Crystal on block and adjustment mechanism in position in the instrument below the collimator. Motion of the crystal and block around the axis bb' is effected by the adjustment knob at B.

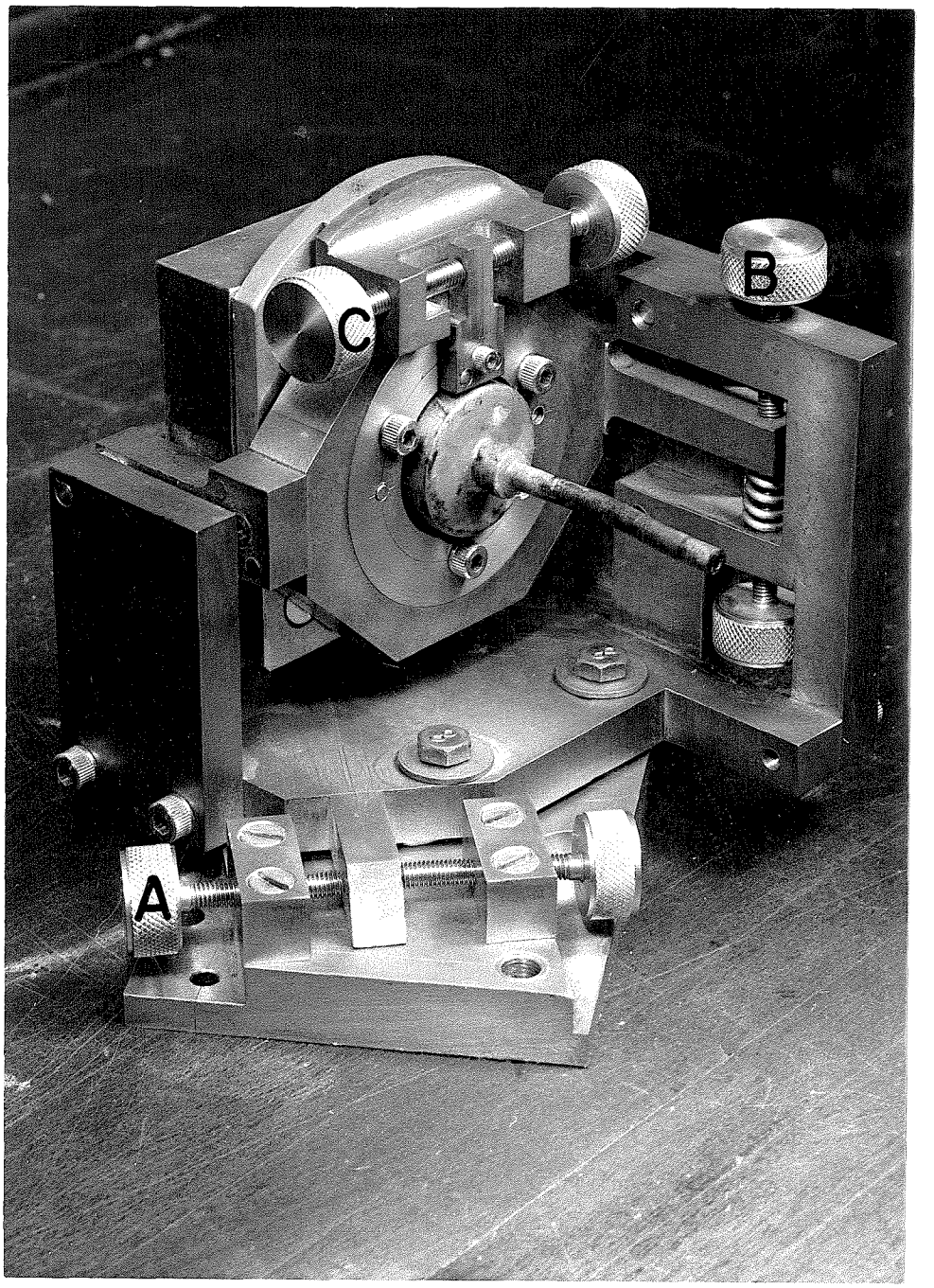

Fig. 15. Crystal block mounting and adjustment mechanism. The knobs at A, B, and C adjust the position of the crystal. See page 25.

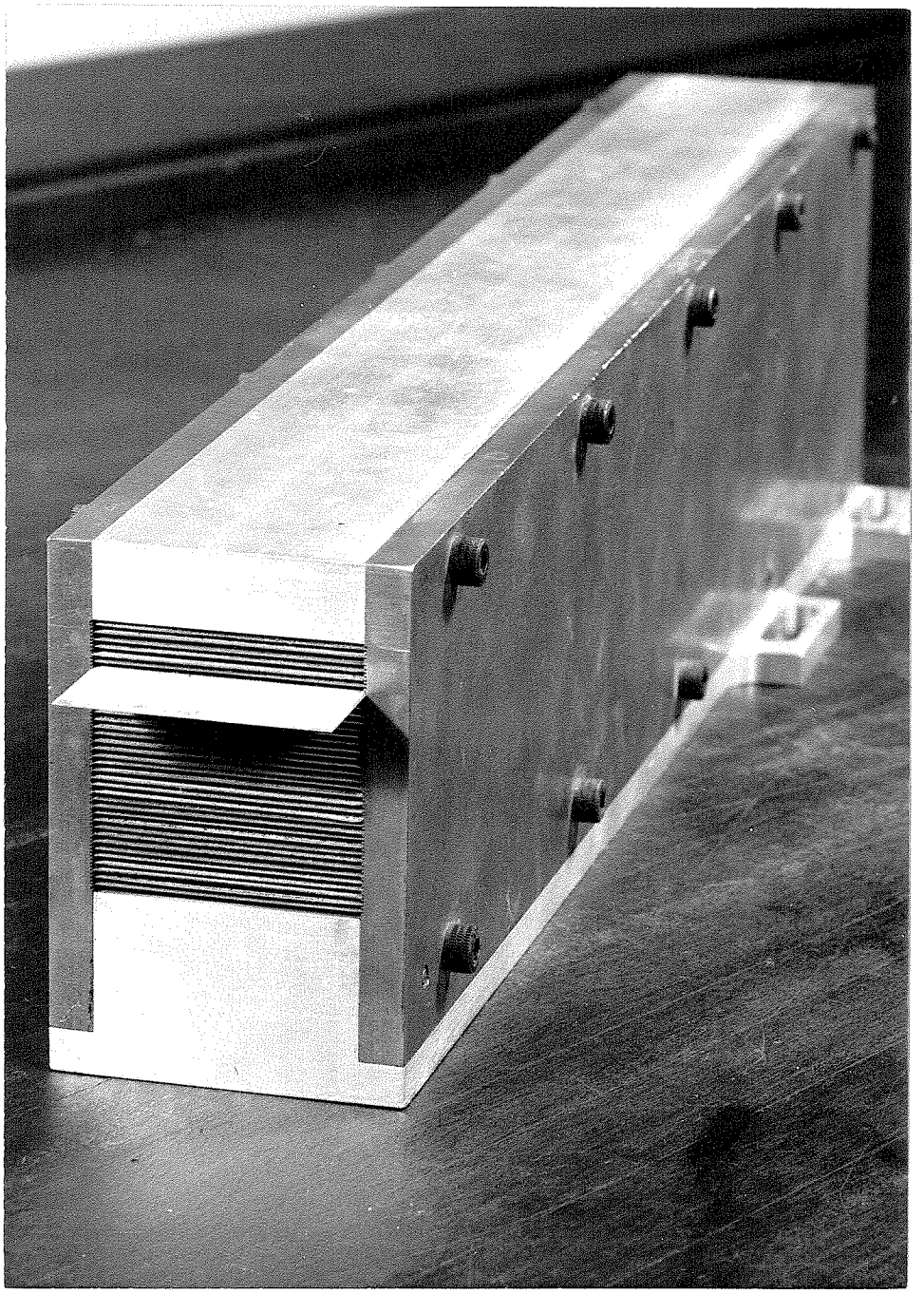

Fig. 16. View of the narrow end of the collimator. One of the vanes is partially pulled out.

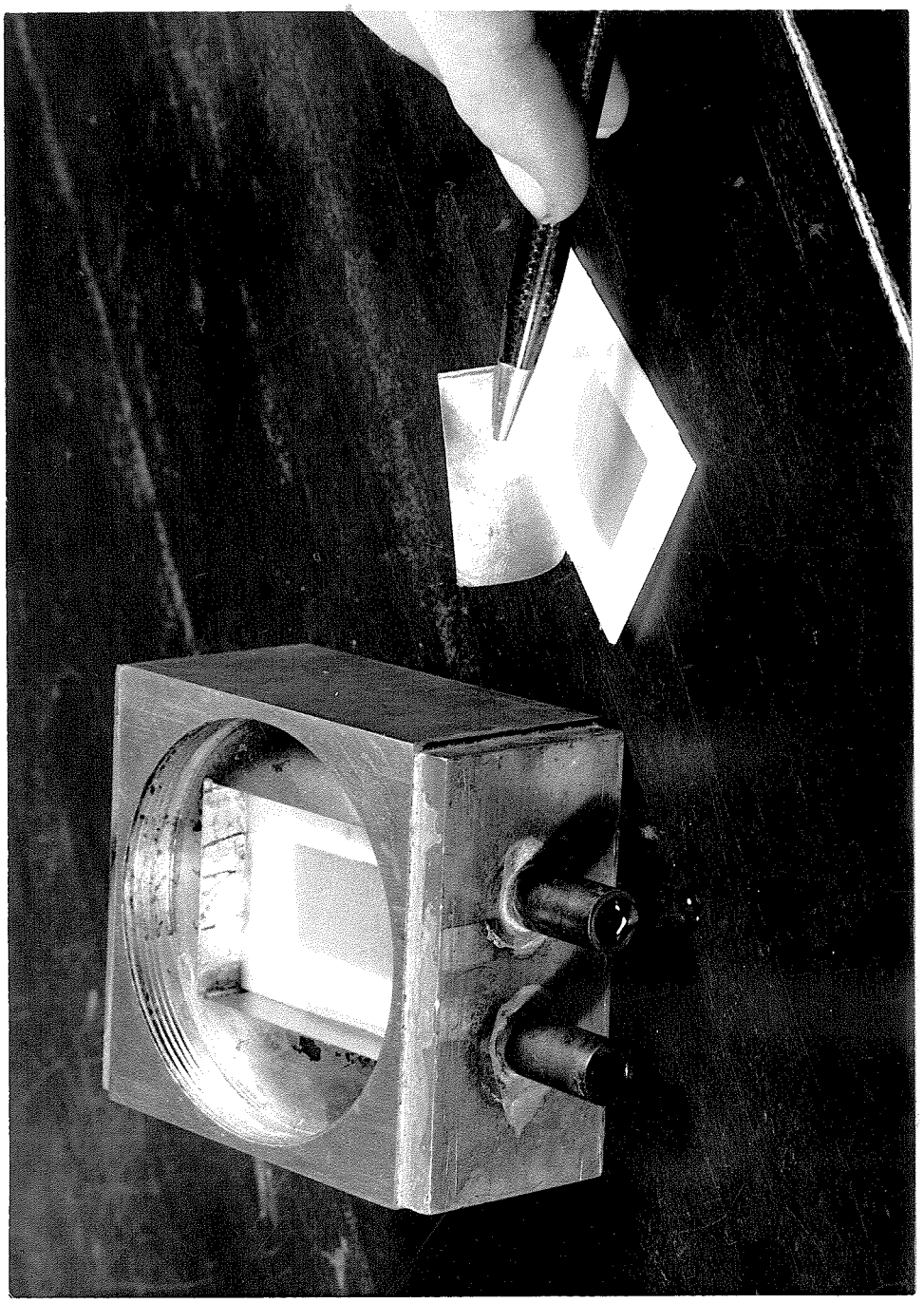

Fig. 17. Sample frame in brass sample frame holder, with another sample frame beside it showing the Parafilm film partially pulled out.

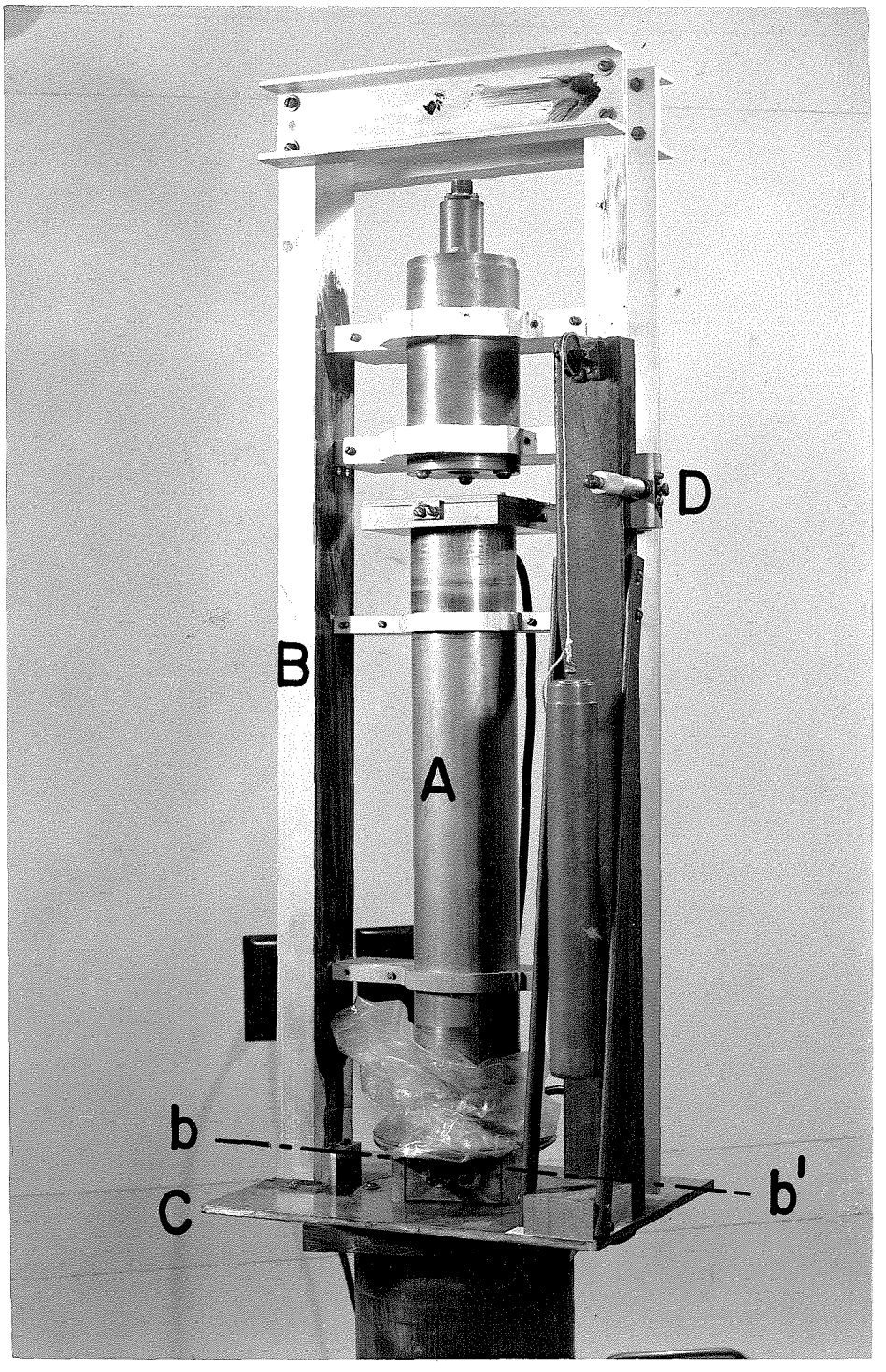

Fig. 18. Geiger counter installation for the second series of ribosome runs. See page 43.

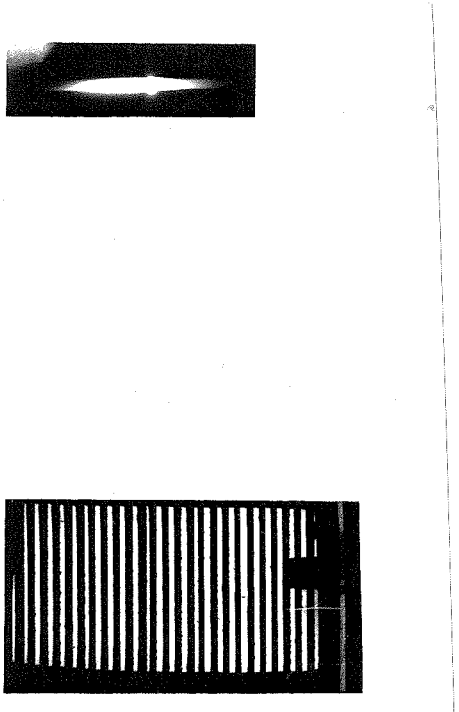

Fig. 19. Above: Photograph of focal spot of approximately 15 minutes' exposure showing results of reflection from the collimator vanes.

Below: Photographic exposure with film in the sample position for maximum sample-to-film distance. Black square is caused by a piece of lead masking off a portion of the crystal where there is a speck of dust between the crystal and the crystal block distorting a small area of the crystal surface. Enlarged 1.5 times.

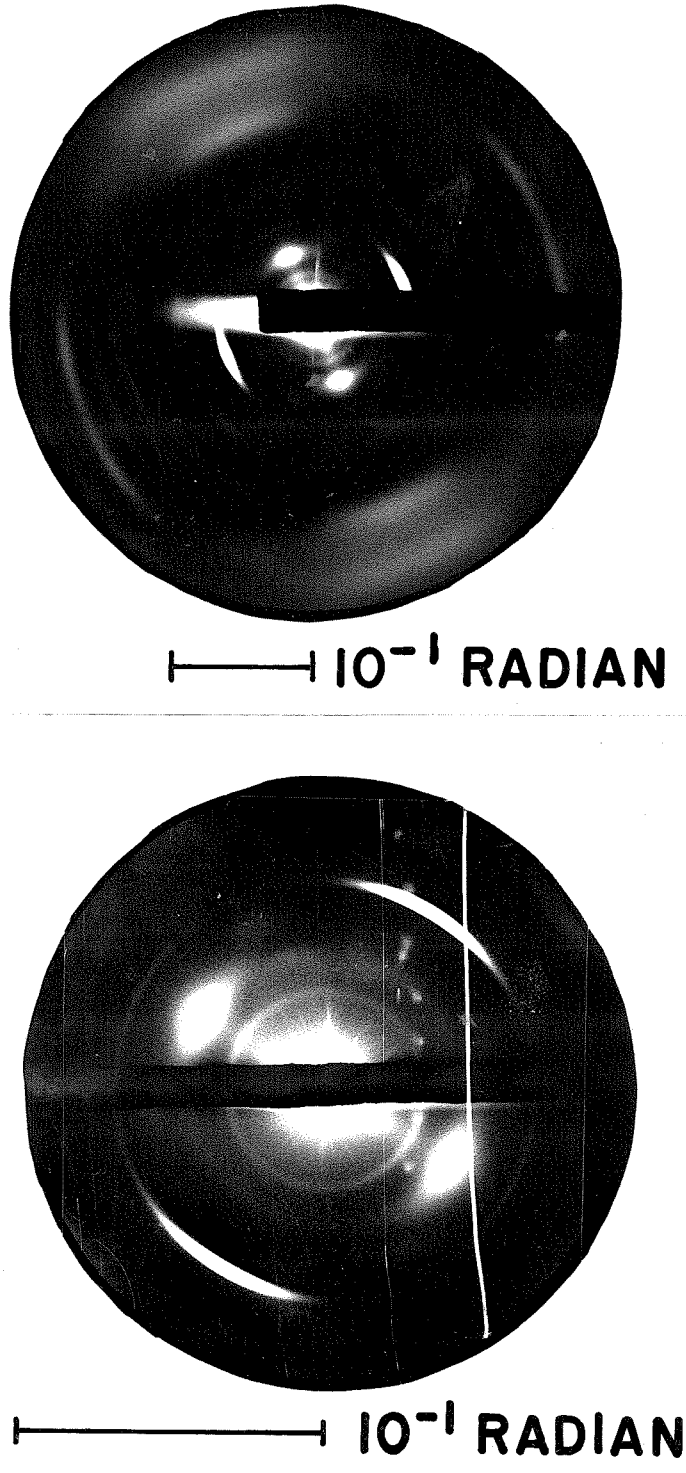

Fig. 20. X-ray scattering patterns of keratin from seagull feathers. The upper exposure was at a sample-to-film distance of 12.5 cm for 34.3 hours. The lower exposure was at a sample-to-film distance of 27 cm for 100.2 hours. Enlarged 1.5 times.

Fig. 21. X-ray scattering patterns of bovine serum albumin on Kodak Medical No-Screen film at a sample-to-film distance of 48 cm. The upper exposure is of a 15% solution for 48.3 hours. The lower exposure is of a 5% solution for 70 hours. Enlarged 1.5 times.

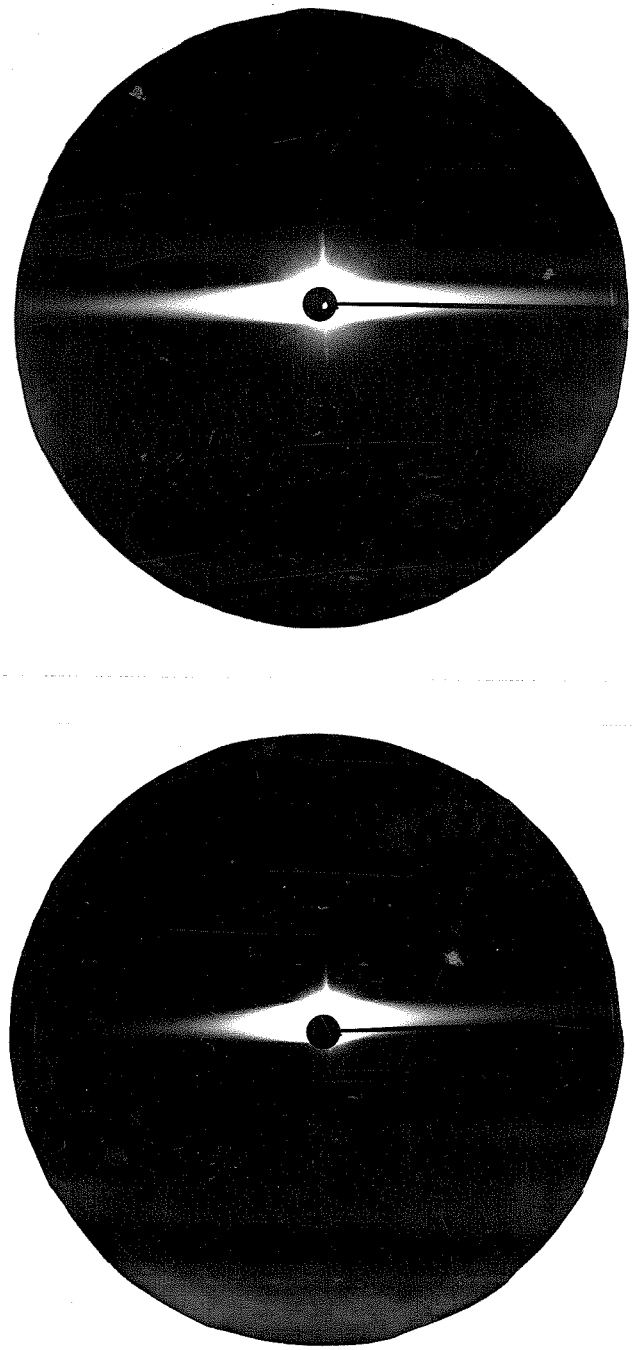

Fig. 22. X-ray scattering patterns of bovine serum albumin on Kodak Medical No-Screen film at a sample-to-film distance of 48 cm. The upper exposure is of 1% solution for 100 hours. The lower exposure is of a background with water for 48.3 hours. Enlarged 1.5 times.